

Hybrid mesoporous aluminosilicate catalysts obtained by non-hydrolytic sol-gel for ethanol dehydration

Ales Styskalik,^{a,b} Imene Kordoghli,^a Claude Poleunis,^a Arnaud Delcorte,^a Zdenek Moravec,^b
Lucie Simonikova,^b Viktor Kanicky,^b Carmela Aprile,^c Luca Fusaro,^c Damien P. Debecker^{*a}

^aInstitute of Condensed Matter and Nanoscience (IMCN), UCLouvain, Place Louis Pasteur 1,
1348 Louvain-La-Neuve, Belgium

^bMasaryk University, Department of Chemistry, Kotlarska 2, CZ-61137 Brno, Czech Republic

^cDepartment of Chemistry, Unit of Nanomaterials Chemistry, University of Namur, 5000 Namur,
Belgium

*Corresponding author (damien.debecker@uclouvain.be).

ABSTRACT

Ethanol dehydration is effectively catalyzed by solid acids, such as HZSM-5, alumina, or silica-alumina. In these catalysts, the amount, nature, and strength of acid sites is believed to determine catalyst activity and stability. However, surface hydrophilicity or hydrophobicity can be suggested as another decisive materials property that can directly influence performance. For example, a more hydrophobic surface might be beneficial in repelling the co-product of the reaction, water. However, these aspects have been studied only scarcely in the context of alcohol dehydration. Here, a series of mesoporous hybrid aluminosilicate materials containing CH_3Si groups was prepared in one pot by non-hydrolytic sol-gel (NHSG). The presence of the methyl groups was verified by IR, solid-state NMR, and ToF-SIMS. Aluminum is mostly incorporated in tetrahedral coordination in the hybrid silica matrix. Two parameters were varied: (i) the aluminum loading (Si:Al ratio) and (ii) the degree of methylation (Si:MeSi ratio). On the one hand, changing the Si:Al ratio had a marked and expected impact on acidity. On the other hand, unexpectedly, the introduction of methyl groups had no clear influence on sample hydrophobicity. Nevertheless, some of the methylated aluminosilicate catalysts markedly outperformed the purely inorganic catalysts and a commercial silica-alumina benchmark. While a direct influence of surface hydrophilicity or hydrophobicity is unlikely, characterization of acidity (IR-pyridine) revealed that the improved performance for hybrid catalysts is correlated with a modification of the acidic properties (higher proportion of Lewis acid sites) caused by the introduction of methyl groups during the sol-gel process. A decisive role of acidity in ethanol dehydration was confirmed by an experiment with delayed addition of the Al precursor in the NHSG synthesis of the hybrid aluminosilicate. This led to a higher Al surface concentration, marked acid sites number increase, and better catalytic performance, even competing with the state of the art HZSM-5 in terms of ethylene yield.

Keywords: non-hydrolytic sol-gel, hybrid aluminosilicate; hydrophobicity; acidity; heterogeneous catalysis; ethanol dehydration

Introduction

Hybrid organic-inorganic materials based on silica have recently attracted considerable attention because of their possible application in catalysis, adsorption, and gas sensing^{1,2}. In the field of heterogeneous catalysis, many publications have reported a beneficial effect of the introduction of organic groups into inorganic catalysts, in terms of catalytic performance. This strategy is especially claimed to be successful when water should be repelled from the surface – e.g. in transesterification of fatty acids, condensation of aldehydes with alcohols, alkylation of phenols, olefin epoxidation, ethyl lactate production from dihydroxyacetone, sugar isomerization, etc.³⁻¹⁰ The higher activity of the hybrid catalysts is often claimed to be related to a higher hydrophobicity.

In some cases, this is supported by quantitative analyses. For example, it was shown by immersion calorimetry, that the grafting of trimethylsilyl groups on the surface of Ti-SBA leads to a decrease of its hydrophilicity.¹¹ The silylated samples were more active, selective, and stable in epoxidation reactions. This was explained by a modulation of the detrimental effect of water on the catalytic reactions (e.g. epoxide ring opening, coordination to Ti catalytic centers and thus their deactivation, etc.). Water molecules were effectively repelled from the hydrophobic catalyst surface and did not interfere with epoxidation.¹¹

Nevertheless, many publications on hybrid catalysts lack some measure of hydrophobicity (i.e. water sorption, competitive sorption of water/toluene mixtures, immersion calorimetry, inverse gas chromatography, or dynamic vapor sorption) and the reported effect of “hydrophobicity” on catalytic activity is only put forward based on the presence of organic groups in the

heterogeneous catalysts. The direct effect of hydrophobicity on catalytic activity, however, is only one of the possible explanations for catalytic performance improvement.

Acid site strength modulation upon organic groups incorporation is another possible effect. For example sulfonic acid sites were shown to become stronger upon grafting of octyltriethoxysilane on the surface of a sulfonated MCM-41 silica.¹² As terminal Si-OH groups are consumed, their hydrogen bonding with $-SO_3H$ groups are disrupted, leaving stronger sulfonic acid moieties with a higher degree of freedom. This in turn led to an improved catalytic performance in butanol esterification with acetic acid.¹² A similar effect of acid site strength increase has been observed for periodic mesoporous organosilica materials as well.³ While catalytic activity was correlated with acid site strength (enhanced by hydrogen bonding diminution), the hydrophilicity of the materials (described by competitive water/toluene mixture adsorption) remained unaffected. It was found that the reported hydrophobicity index strongly depends on the $-SO_3H$ content (highly polar and thus hydrophilic), while the introduction of “hydrophobic” organic groups provoked only minor changes.³

The dehydration of bioalcohols – e.g. bioethanol – is an important catalytic reaction in the perspective of the development of a bio-based industry.¹³⁻¹⁷ Traditional catalysts employed in this reaction are alumina, silica-alumina, and HZSM-5.^{18,19} Each of these systems come with their own limitations: only moderate activity in the case of Al_2O_3 and silica-alumina, and rapid deactivation by coking in the case of zeolite catalysts. Application of hydrophobic hybrid materials might be beneficial in the dehydration reaction, because the surface properties (mainly hydrophilicity and acidity) can in principle be fine-tuned by the presence of the organic moieties. However, the use of hybrid materials to boost catalyst activity, selectivity or stability

has been reported only scarcely in the case of alcohol dehydration.^{8,20} As an example, organically modified sulfonated silica materials have been reported as efficient catalysts for butanol dehydration to dibutylether in the liquid phase.^{21,22} Some improvements in catalytic activity were observed upon organic groups introduction; however, a clear and direct influence of “hydrophobicity” of applied catalysts (derived from heat of H₂O adsorption²¹ and water/hexane sorption capacity²², respectively) on their catalytic activity has not been proved.^{21,22} On the contrary, van Grieken et al. have shown, that propylsulfonic acid modified SBA-15 adsorbs less water with a lower strength in comparison to arenesulfonic acid modified SBA-15 (TPD-H₂O).²³ Both catalysts displayed similar numbers of acid sites. The catalyst showing lower hydrophilicity exhibited a better performance in etherification of benzylalcohols with 1-hexanol (dehydration reaction).²³ To the best of our knowledge those are the only reports studying the relationship between hydrophobicity and catalytic performance in alcohol dehydration.

We have recently reported the synthesis of various highly porous hybrid metallosilicates by non-hydrolytic sol-gel (NHSG), their characterization, gas phase hydrothermal stability, and catalytic performance in ethanol dehydration.²⁴ The aluminosilicates based on xylylene bridged hybrid silica (O_{1.5}Si-CH₂-C₆H₄-CH₂-O_{1.5}; silsesquioxanes) were thermally stable up to 350 °C and active in ethanol dehydration. However, their performance did not compete with the pure inorganic benchmark catalysts.

Moving further, here we focus on the synthesis and characterization of hybrid metallosilicates and their application in ethanol dehydration with the intent to (i) follow sample hydrophobicity, (ii) elucidate its effect on catalytic performance and (iii) develop materials with enhanced

performance. We focus on the incorporation of methyl groups bound to silica. Their content ranges from 0 to 10 mol% (based on total Si molar amount) thus avoiding high organic groups concentration, which has been shown ineffective.²⁴ These highly porous hybrid metallosilicate catalysts were prepared in one step by non-hydrolytic sol-gel chemistry (NHSG)^{25–27}. The introduction of organic groups and of the metal took place directly during the polycondensation reactions, using the alkyl halide elimination route. By changing the Si:Al ratio or by delaying the addition of the Al precursor into the sol-gel reaction mixture, we show we are able to control the number of accessible acid sites and that this is strongly correlated with activity. Furthermore, we demonstrate the successful introduction of methyl groups, and we disclose a counter-intuitive impact of these groups on the hydrophobicity and on the catalytic behavior. From these observations, we present an integrated view on the key parameters that influence catalytic performance in ethanol dehydration. We use the teachings of this study to design highly active hybrid aluminosilicate catalysts.

Experimental

General. All manipulations were performed under high vacuum or dry N₂ atmospheres using Schlenk techniques or in a dry box with H₂O and O₂ levels below 1 ppm. Diisopropylether and benzene-d₆ were dried over Na metal. CH₂Cl₂ was dried with P₄O₁₀. All solvents were distilled, and stored in a glovebox over molecular sieves. Aluminum chloride (ABCR, AlCl₃, 99.999 %), silicon tetrachloride (Sigma, SiCl₄, 99 %), and methyltrichlorosilane (Sigma, CH₃SiCl₃, 99 %) were stored in a glovebox and used as received. Ethanol absolute (AnalaR NORMAPUR, 99.95 %) was used as received. Silica-alumina catalyst support (grade 135, S_ABET = 600 m² g⁻¹, V_{total} =

0.76 cm³ g⁻¹, Si:Al ratio ~8, **SACS**) was purchased from Sigma-Aldrich. ZSM-5 zeolite in ammonium form ($S_{\text{BET}} = 400 \text{ m}^2 \text{ g}^{-1}$, Si:Al ratio ~15) was purchased from Alfa Aesar and calcined at 500 °C in order to transform it to H⁺ form (**HZSM-5**). $\gamma\text{-Al}_2\text{O}_3$ (3 μ APS powder, $S_{\text{BET}} = 80\text{-}120 \text{ m}^2 \text{ g}^{-1}$) was purchased from Alfa Aesar.

Characterization. Transmission IR spectra (4000–400 cm⁻¹) were recorded on a Bruker Equinox 55 spectrometer from KBr pellets or on a Bruker Alpha-Platinum ATR system. The same instrument was used – in combination with pyridine adsorption – to quantify acid sites.²⁸ Wafers based on ca. 30 mg of analyzed sample were pressed and evacuated at 350 °C at $\approx 10^{-4}$ Torr overnight. Then pyridine was adsorbed at its autogenous pressure at RT for 30 min. Physisorbed pyridine was removed by evacuation at 150 °C at $\approx 10^{-4}$ Torr for 2 hrs and IR spectra were collected. Molar extinction coefficients according to Emeis were used for calculations for absorption bands at 1455 cm⁻¹ (Lewis acid sites) and at 1545 cm⁻¹ (Brønsted acid sites).²⁸ Strength of acid sites was estimated by further evacuation/IR measurement steps at 250 and 350 °C. . Thermal analysis (TG/DSC) was performed on a Mettler Toledo TGA/DSC 3+ apparatus in the stream of air (100 cm³ min⁻¹) with a temperature ramp of 5 °C min⁻¹ to 1000 °C, in an alumina crucible. Surface areas (SA) and pore volumes were determined by nitrogen adsorption at 77.4 K by volumetric techniques^{29,30} on a Tristar 3000 instrument (Micromeritics, USA). Prior to measurement, the samples were degassed at 150 °C for at least 8 hrs. The specific surface area was determined by the multipoint BET method with at least five data points with relative pressures between 0.05 and 0.30. Water adsorption was performed on a 3Flex instrument (Micromeritics) and Autosorb-iQ-MP (Quantachrome) at room temperature ($p_0 = 21$ Torr). Prior to measurement, the samples were degassed at 150 °C for at least 8 hrs. The ratio of volume of

adsorbed liquid H₂O (calculated from H₂O adsorption) and volume of adsorbed liquid N₂ (calculated from N₂ physisorption) at $p/p_0 = 0.3$ was denoted $X_{0.3}$ and taken as a measure of hydrophilicity (“hydrophilicity index”) similar to reports by Gounder et al.⁹, Olson et al.³¹ and Thommes et al.³². Aluminum and silicon contents were determined on an ICP optical emission spectrometer iCAP 6500 Duo (Thermo, UK) equipped with a solid-state generator with a frequency of 27.12 MHz and a maximum power input of 1350 W. The measurements of Al were performed at 308.2, 394.4, and 396.1 nm. For Si analysis, wavelengths 212.4 and 251.6 nm were used. Solution NMR spectra were recorded on a Bruker 300 MHz NMR spectrometer at frequencies 299.8 MHz for proton and 75.4 MHz for carbon with deuterated solvents as the external lock. The proton and carbon NMR spectra were referenced to the residual proton signals or carbon resonances of benzene-d₆ (7.15 and 128.0 ppm, respectively). Solid-state ²⁷Al, ²⁹Si, and ¹³C solid state magic angle spinning (MAS) NMR spectra were acquired on Bruker Avance-500 NMR spectrometer with a 4 mm CP-MAS Bruker probe at frequencies 99.4 MHz for silicon, 130.3 MHz for aluminum, and 125.8 MHz for carbon. MAS rates were 8 kHz for ²⁹Si and ¹³C (CP)MAS and 10 kHz for ²⁷Al MAS spectra. Quantitative ²⁹Si MAS spectra were recorded using a 300 s relaxation delay, a 3 μs (90°) excitation pulse, and a 52 ms acquisition time. Chemical shifts were referenced externally to ²⁹Si δ[3-(trimethylsilyl)-1-propanesulfonic acid sodium salt (DSS)]: 1.53 ppm; ¹³C δ[adamantane] 38.68 ppm; ²⁷Al δ [[Al(H₂O)₆]³⁺ (aq. solution)]: 0.0 ppm. The quantitative analysis of ²⁹Si MAS NMR spectra (exponential line broadening value = 0) was performed as follows: (i) phase correction; (ii) baseline correction using least squares method; (iii) deconvolution of signals to T¹, T², T³, Q², Q³, and Q⁴ peaks with 100 % Gaussian shape until RMS deviation characterizing the fit between calculated and measured data was

below 0.05; (iv) integration. The relative integrated areas of mentioned peaks were used to calculate the percentage of T sites. X-Ray photoelectron spectroscopy (XPS) measurements were carried out on a SSI X probe spectrometer (model SSI 100, Surface Science Laboratories, Mountain View, CA) equipped with a monochromatized Al-K α radiation (1486 eV). The sample powders, pressed in small stainless troughs of 4 mm diameter, were placed on an insulating home-made ceramic carousel. The pressure in the analysis chamber was around 10^{-6} Pa. The analyzed area was approximately 1.4 mm^2 and the pass energy was set at 150 eV. The C1s peak of carbon has been fixed to 284.8 eV to set the binding energy scale ³³. Data treatment was performed with the CasaXPS program (Casa Software Ltd, UK) and spectra were decomposed with the least squares fitting routine provided by the software with a Gaussian/Lorentzian (85/15) product function and after baseline was subtracted. Time of flight secondary ion mass spectrometry (ToF-SIMS) analyses conducted with a TOF.SIMS⁵ instrument (IONTOF GmbH, Münster, Germany). A pulsed Bi⁵⁺ metal ion source was used to produce a primary beam using an acceleration voltage of 30 kV. An AC target current of 0.07 pA with a bunched pulse width lower than 1 ns was used. Both positive and negative secondary ion species were analysed. Mass spectra were obtained by scanning the primary ion beam over a $250 \times 250 \mu\text{m}^2$ area. The total primary ion beam dose for each analysed area was always kept below $5 \cdot 10^{10}$ ions cm^{-2} , ensuring static conditions. Lateral resolution of $\sim 3 \mu\text{m}$ and mass resolution $m/\Delta m > 4000$ at 29 m/z were maintained for positive and negative mass spectra acquisition. Charge compensation was conducted using an interlaced electron flood gun (kinetic energy = 20 eV). All data analyses were carried out with the software supplied by the instrument manufacturer, SurfaceLab (version 6.5). Sample powders were pressed onto the adhesive part of Post-it[®]

papers. Water contact angle measurements were performed on See System apparatus from Advex Instruments. Fine catalyst powders were pressed into the form of pellets at 5 MPa. Water contact angles were measured by the sessile drop method at 25 °C with five to ten measurements at different positions of the pellet for each sample.

Xerogel synthesis. In a typical synthesis, 6.120 g (59.89 mmol) diisopropylether (DIPE), 0.2659 g (1.779 mmol) methyltrichlorosilane, and 4.566 g (26.87 mmol) silicon tetrachloride were loaded in an autoclave equipped with 45 cm³ CH₂Cl₂ in a glove box. 0.2429 g (1.822 mmol) AlCl₃ (neat) was directly added to this reaction mixture with vigorous stirring and stirred at RT until complete dissolution (5–10 min). No surfactant was used in the synthesis. The autoclave was sealed and kept in an oven at 110 °C for 72 hrs for gelation (Eqn. 1). After cooling down, the autoclave was put back into the glovebox, opened and the gel was transferred into a Schlenk vessel. The gel was then dried under vacuum at 60 °C overnight in order to remove the solvent and volatile condensation product (isopropylchloride). The resulting powder was calcined in flow of dry air at 300 °C (1 °C min⁻¹, 5 hrs) yielding a brown xerogel. This sample is called “**15Si-1MeSi-1Al**”; the name explicitly shows that the methylation degree corresponds to 1 methylated Si atom for 15 non-methylated Si atoms, and the Si:Al ratio is 16. From this formulation, 2 parameters were varied at the time of synthesis: (i) aluminum loading (samples **15Si-1MeSi-0.25Al**, **15Si-1MeSi-0.5Al**, and **15Si-1MeSi-2Al**); (ii) methyl groups loading (samples **14Si-2MeSi-1Al** and **13Si-3MeSi-1Al**). Pure inorganic benchmark catalyst with the same Si:Al nominal ratio was prepared in the same way utilising SiCl₄ solely as a silicon precursor (**16Si-1Al**). Finally in one synthesis, the addition of 90 % of the required amount of AlCl₃ was delayed

for 8hrs in order to increase the concentration of aluminum in the surface layer of the catalyst (**15Si-1MeSi-1DAI**). Precise reactant masses used in the syntheses can be found in Table 1S.



Spectroscopic characterization data (IR and NMR). Complete summary can be found in the supporting material to this manuscript (ESI). These may be accessed via journal website.

Catalytic dehydration of ethanol. The calcined xerogel catalysts (0.192 g, sieved in the 0.20–0.40 mm particle size range) were diluted with glass beads (0.5-1 mm) in order to keep the volume of the catalyst bed constant. The void space of the reactor was filled with silica beads. Catalytic testing was carried out by injecting 0.212 g h⁻¹ of absolute ethanol by means of NE-300 syringe pump in a 40 cm³ min⁻¹ flow of N₂ (4.4 mol% of ethanol in N₂). The tests were carried out at atmospheric pressure, WHSV = 1.1 h⁻¹. Temperature was varied stepwise in the range from 205 to 310 °C by steps of 35 °C. One step consisted of (i) heating ramp (5 °C min⁻¹) and stabilization at the set temperature (21 min) and (ii) steady temperature state (56 min). The analysis of the effluent gas was carried out by a VARIAN 3800 Gas Chromatograph (8 injections at each temperature) equipped with a flame ionization detector (FID) and a Cydex B column (25 m long, internal diameter 0.22 mm, film thickness 0.25 μm).

Results and discussion

As compared to a pristine mesoporous aluminosilicate catalyst, some hybrid catalysts obtained through the introduction of methyl groups showed a higher performance. Before elucidating the effect of methylation (see Section 3.2 Effect of methylation), we identify the decisive parameters that dictate the catalytic behavior of the hybrid catalysts (Section 3.1 Si:Al ratio). Finally, based on the knowledge gained in Section 3.1 and 3.2, we present a strategy of delaying Al addition into the reaction mixture in order to increase the surface Al concentration which leads to a marked improvement in catalytic performance (Section 3.3).

Effect of Si:Al ratio

Hybrid aluminosilicate samples with pending methyl groups on one out of 16 Si atoms, and with different Al loadings (**15Si-1MeSi-0.25Al**, **15Si-1MeSi-0.5Al**, **15Si-1MeSi-1Al**, and **15Si-1MeSi-2Al**) were prepared by NHSG. The nominal Si:Al ratio was ranging from 64 to 8 and ICP-OES analysis data correlated well with the nominal values (Table 1). The Si:Al ratios in the surface layer (as determined by XPS) were, on the other hand, somewhat higher than in the bulk, as typically observed for metallosilicate prepared by the alkyl halide elimination route (ether route, Eqn. 1). NHSG is known to produce mixed metal oxides with good textural properties (even without requiring the use of a sacrificial templating agent).²⁵⁻²⁷ Here, the synthetic procedure is similar to the protocol typically proposed for purely inorganic metallosilicates³⁴⁻³⁸, but including a methylated silicon precursor (methyltrichlorosilane).^{7,39} Also, the calcination temperature was decreased from 500 °C to 300 °C in order to prevent organic groups oxidation in hybrid materials. According to TG analysis the materials are a relatively stable at this temperature, and the progressive oxidation of methyl groups is observed between 350 and 700 °C (Fig. 1S).

Table 1: Characterization of NHSG prepared samples with different Al loading: Si:Al ratio (theoretical^a, bulk – ICP-OES and surface – XPS), surface area, pore volume, and average pore size estimated from N₂ physisorption experiments.

Sample	Si:Al ratio	S _{ABET} (m ² g ⁻¹)	V _{total} (cm ³ g ⁻¹)	D (nm)
	Theor ^a /ICP/XPS (-)			
15Si-1MeSi-0.25Al	61.8/69.3/72.6	390	0.71	7.3
15Si-1MeSi-0.5Al	31.7/33.2/33.5	360	1.1	12
15Si-1MeSi-1Al	15.7/16.3/24.2	270	0.75	11
15Si-1MeSi-2Al	8.0/6.8/15.0	90	0.21	9.9

^aThe nominal Si:Al ratio is 16 (64, 32, 8); the theoretical value presented in the table is the value calculated from the precise masses of reactants introduced during the synthesis (n_{Si} , n_{RSi} , n_{Al} , n_{DIPE}), as presented in Table 1S.

Textural properties were analyzed by N₂ adsorption-desorption experiments (Fig. 1, Table 1).

Specific surface area (S_{ABET}) was the highest (390 m² g⁻¹) for the sample with the lowest Al loading (**15Si-1MeSi-0.25Al**) and was decreasing with increasing Al content. An abrupt loss of specific surface area was observed for the sample with the highest Al loading (**15Si-1MeSi-2Al**); S_{ABET} dropped down to 90 m² g⁻¹. Pore volumes (V_{total}) were very high for most catalysts, up to 1.1 cm³ g⁻¹ for catalyst **15Si-1MeSi-0.5Al**. Only the catalyst with the highest Al loading (**15Si-1MeSi-2Al**) showed a relatively low pore volume (0.21 cm³ g⁻¹). The average pore diameters were high for all samples (7–12 nm). T-plot analyses indicated that micropores formed only a very small fraction of the total pore volume (0–6 %) of the samples. The fact that the steep hysteresis loop is located at high partial pressures (0.8–1.0 p/p₀) suggests that a significant fraction of porosity originates from interparticle voids.⁴⁰

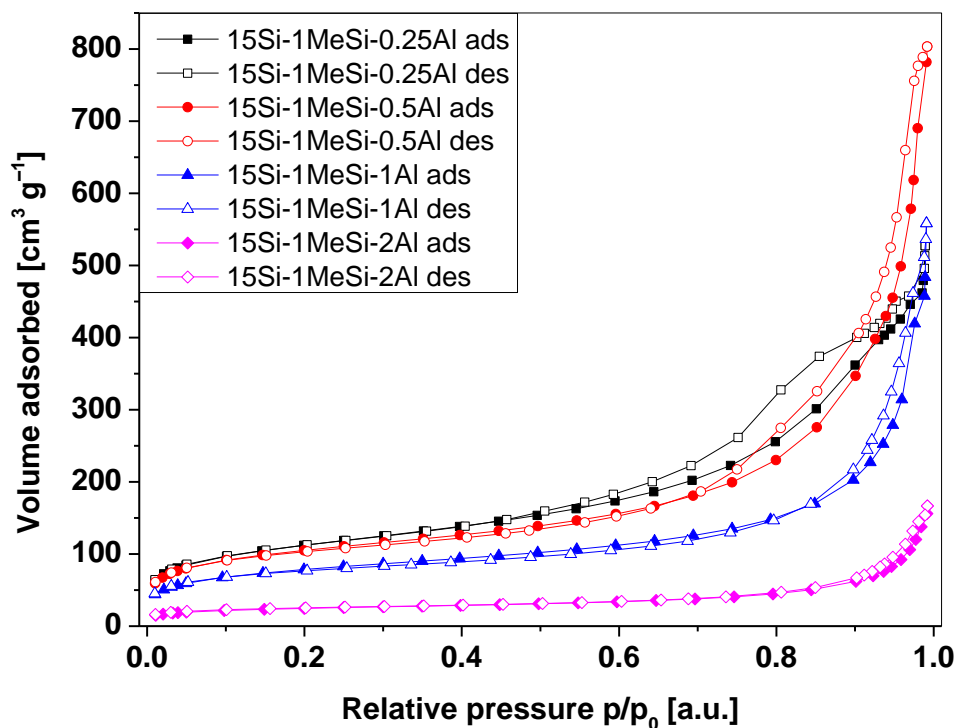


Fig. 1: N₂ physisorption measurements performed on aluminosilicate samples with different Si:Al ratios.

IR spectra were very similar for all four samples (Fig. 2S). The most intense absorption band at 1050–1065 cm⁻¹ was ascribed to the asymmetric stretching vibration of Si–O–Si. The position of this band, at a lower wavenumber in comparison to pure silica (1200 cm⁻¹), is explained by the presence of Si–O–Al bridges.^{41–43} Other absorption bands of lower intensity were observed at 570–580, 798–805, and 925–955 cm⁻¹ and can be assigned to Si–O–Si deformation vibration, symmetric Si–O–Si stretching vibration, and Si–O–H stretching vibration, respectively.⁴⁴ Importantly, a band was observed in all spectra at 1281 cm⁻¹, originating from CH₃Si symmetric deformation vibration.⁴⁵ This confirms the successful incorporation of methyl groups within the silica network. This is also corroborated independently by solid state NMR and ToF-SIMS (vide infra).

^{29}Si CPMAS NMR spectra were also very similar for these four catalysts prepared by NHSG. The main signal was observed at -101 ppm with two shoulders of lower intensity at -91 and -112 ppm (Fig. 3S). These signals were ascribed to $\text{Si}(\text{OSi})_3(\text{OH/OAl})$ (Q3), $\text{Si}(\text{OSi})_2(\text{OH/OAl})_2$ (Q2), and $\text{Si}(\text{OSi})_4$ (Q4), respectively.⁴⁶ A broad signal of lower intensity was observed in the range from 42 to 69 ppm. It comes from T species and can be considered as a combination of two contributions at -55 ($\text{CH}_3\text{Si}(\text{OSi})_2\text{OH/OAl}$, T2) and -64 ppm ($\text{CH}_3\text{Si}(\text{OSi})_3$, T3).^{24,47} NMR analyses thus confirmed that the organic groups were successfully incorporated within the aluminosilicate matrices. The amount of methyl groups preserved during the synthesis and calcination was estimated with the help of quantitative ^{29}Si MAS NMR experiments. For **15Si-1MeSi-1Al**, ca. 55 % of organic groups was preserved (see Section 3.3 Effect of methylation).

^{27}Al MAS NMR spectra (Fig. 2, left) showed always the most intense peak for Al in tetrahedral coordination at 50 – 54 ppm confirming a good incorporation of aluminum into the silicate matrices. The broadening of this contribution in comparison to typical signal of AlO_4 moieties in zeolites could be attributed to the amorphous nature of the silica walls hence to the presence of tetrahedral Al in slightly different distorted geometry.⁴⁶ All NHSG prepared samples exhibited a small amount of AlO_5 species as well, based on the presence of a shoulder at ca. 25 ppm.⁴⁸ Finally, octahedrally coordinated Al atoms were also observed (signal at 0 ppm). The amount of octahedrally coordinated Al atoms was rising with increasing Al loading. Interestingly, the aluminosilicates with low Al loading (**15Si-1MeSi-0.25Al** and **15Si-1MeSi-0.5Al**) displayed very sharp signal around 0 ppm indicating presence of some mobile octahedrally coordinated Al species. These were tentatively attributed to loosely bound surface Al moieties with their coordination sphere filled with water molecules.³⁸

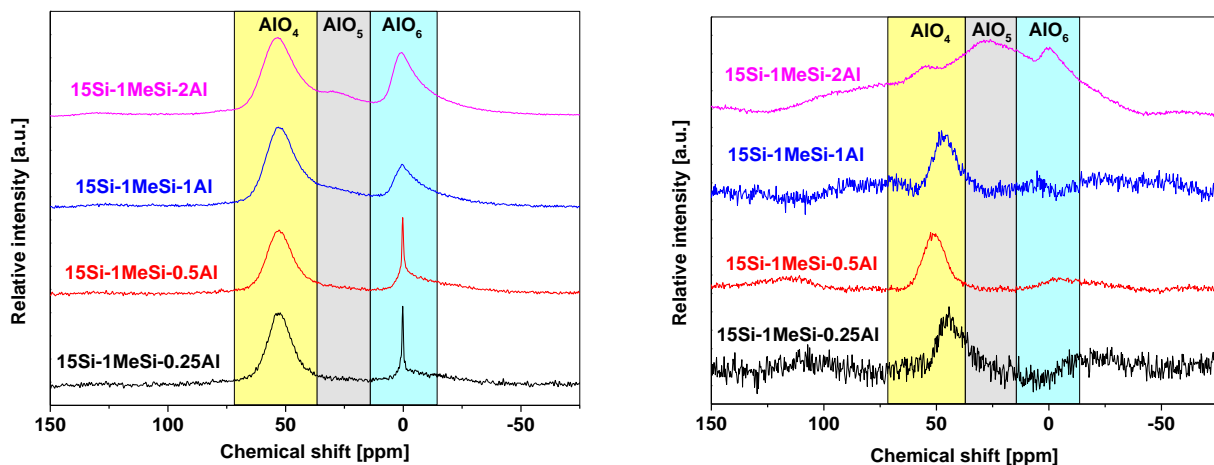


Fig. 2: ^{27}Al MAS NMR spectra of NHSG prepared samples with different Al loading. Left: Samples exposed to ambient atmosphere (hydrated); Right: Dehydrated samples with adsorbed pyridine.

To confirm this hypothesis and gain a deeper insight into structural motifs present in the catalysts, we performed additional ^{27}Al MAS NMR analyses on dehydrated samples (evacuated at 150 °C, overnight) which were consequently contacted with pyridine. It was found that this treatment led to the complete disappearance of AlO_6 and AlO_5 species for **15Si-1MeSi-0.25Al**, **15Si-1MeSi-0.5Al**, and **15Si-1MeSi-1Al** (Fig 2, right). Interestingly, the coordination of water molecules was fully and rapidly reversible on dehydrated samples (if no pyridine adsorbed): degassed aluminosilicate catalyst exposed to ambient atmosphere for 10 min exhibited ^{27}Al MAS NMR spectrum identical to the one before evacuation. Similar behavior was observed for some zeolites as well; it indicates that NHSG prepared catalysts with Si:Al ratios up to 16 do not contain any extra-framework alumina clusters. Octahedrally coordinated Al atoms observed in these samples exposed to ambient atmosphere are in fact isolated Al species able to bind H_2O molecules from air moisture.^{49–51} The sample with the highest Al loading, however, does contain

some extra-framework species, as attested by the persistence of the signal at 0 ppm upon dehydration and pyridine adsorption (Fig. 2 right).

The amount of acid sites was estimated by pyridine adsorption combined with IR spectroscopy (Table 2, Fig. 4S–6S).²⁸ The total number was steadily rising with increasing Al content up to the sample **15Si-1MeSi-1Al**. The number of accessible acid sites however dropped when further increasing the Al content in catalyst **15Si-1MeSi-2Al**. This can be attributed to the stark decrease of specific surface area in this sample. The presence of AlO₆ species (extra-framework alumina clusters) in this sample could decrease the acidity as well.

Table 2: Amount, strength, and nature of acid sites in NHSG prepared aluminosilicates by pyridine adsorption combined with IR spectroscopy.

Sample	Total acid sites (mmol g ⁻¹)	B/L ratio (-)	Acid sites after desorption at 350 °C ^a (%)	B/L ratio ^a (-)
15Si-1MeSi-0.25Al	0.014	0.49	60	0.38
15Si-1MeSi-0.5Al	0.028	0.49	63	0.13
15Si-1MeSi-1Al	0.035	0.40	70	0.16
15Si-1MeSi-2Al	0.022	0.64	64	0.42

^aThe fraction of acid sites preserved after desorption at 350 °C is used as an indication of acid site strength.

Both Brønsted and Lewis acid sites are present in all samples; the B/L ratio ranges from 0.40 to 0.64. A relatively high fraction of pyridine (60–70 %) stays adsorbed at the acid sites after evacuation at 350 °C. However, the B/L ratio drops in all cases upon evacuation at high temperature (ranging from 0.13 to 0.42), showing that Brønsted acid sites display lower strength in comparison to Lewis acid sites. Similar characteristics were observed for purely inorganic aluminosilicates prepared by NHSG and calcined at 500 °C.³⁸ Comparison with commercial silica-alumina (amorphous) and zeolite HZSM-5 enabled to describe the acidity of the samples as being intermediate between commercial silica-alumina (mostly weak Lewis acid

sites) and HZSM-5 (mostly strong Brønsted acid sites) thanks to a good homogeneity of Si/Al mixing in NHSG prepared aluminosilicates.³⁸

H₂O adsorption isotherms were obtained to probe the hydrophilic/hydrophobic properties of prepared materials (Fig. 3, 7S and 8S). While the high pressure region (p/p_0 close to 1) represents the pore filling with water (where the water-water interaction governs the adsorption), the low pressure region relies mainly on water-adsorbent interaction (if the adsorbent is sufficiently hydrophilic).⁵² The isotherm shapes at the low pressure region for all tested materials are very similar and correspond to hydrophilic materials (steep increase of adsorbed H₂O volume at $p/p_0 < 0.1$) (Fig. 7S). The volume of adsorbed water at low to medium p/p_0 on aluminosilicate catalysts clearly follows the Al content – the higher the Al content, the more H₂O molecules adsorbed. As suggested in the literature^{9,31,32}, a measure of hydrophilicity can be obtained from H₂O and N₂ sorption data by comparing the volume of adsorbed H₂O to the volume of adsorbed N₂ at given p/p_0 values (both adsorbates being considered as in liquid phase). The ratio obtained at $p/p_0 = 0.3$ is shown in Fig. 3, and ratios obtained over the whole range of p/p_0 are plotted in Fig. 8S). It appears clearly that the hydrophilicity follows the Al content in the whole range of relative pressure (Fig. 8S). This observation is in line with numerous reports on water sorption on zeolites with varying Al content and can be explained by the fact that the Al atoms incorporated within silica matrices bring polar Si–O–Al bonds and hydrophilic acid sites.^{31,32,52,53} It should be kept in mind, however, that the textural properties (surface area, proportion of micropores, size and shape of pores) vary quite significantly when changing the Si:Al ratio. This may influence the relative adsorption of N₂ and H₂O at a given pressure and somewhat bias the estimation of hydrophilicity.

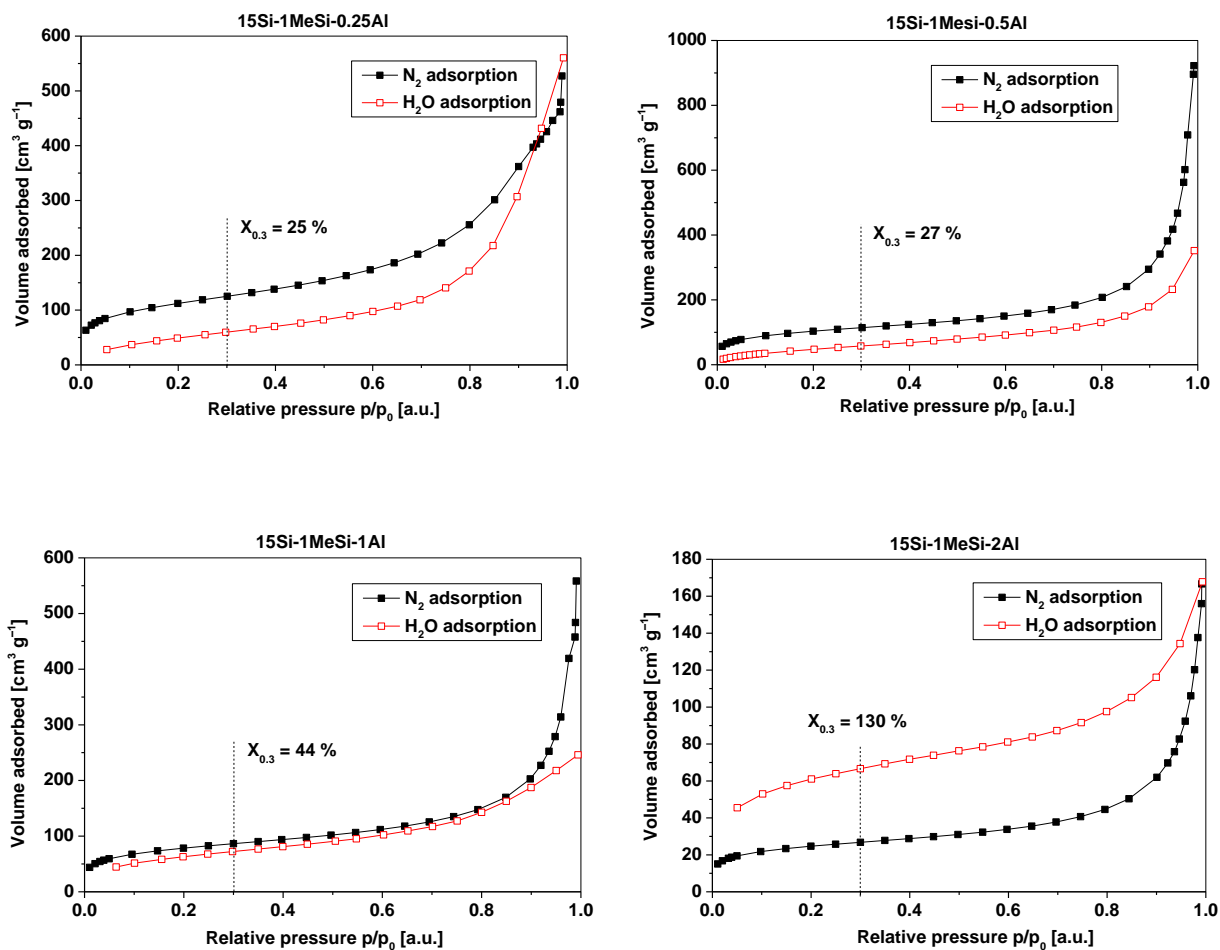


Fig. 3: Comparison of N₂ (solid symbols) and H₂O (open symbols) adsorption isotherms for samples with different Si:Al ratio. „Hydrophilicity index“ X_{0.3} was calculated as a ratio of volume of adsorbed liquid H₂O and volume of adsorbed liquid N₂ at 0.3 p/p₀³².

Thus, the water sorption experiments were complemented by water contact angle measurements on pellets pressed from aluminosilicate catalysts exposed to ambient atmosphere (i.e. hydrated).⁵⁴⁻⁵⁶ Such measurements are considered to be relatively ill-suited for powdery materials, as the contact angle can be influenced by the particles morphology and

texture, and by the roughness of the analyzed sample.⁵⁷ Here, we managed to obtain repeatable results by preparing smooth sample pellets (see Experimental section) and repeating the experiment 5 to 10 times. Unlike the water sorption measurements, no trend was observed in the contact angle method: samples with different Si:Al ratio were all highly hydrophilic with a low water contact angle, ranging from 20.0 ± 2.0 to 26.7 ± 1.6 ° only (Fig. 9S).

The hybrid aluminosilicate catalysts prepared by NHSG were tested in the gas-phase ethanol dehydration in the temperature range between 205 and 310 °C. The major products of the catalytic reaction were ethylene and diethylether with carbon balances reaching 90–105 % (Fig. 4, Table 2S). No other products were observed (neither acetaldehyde, nor propene, nor butenes, as frequently encountered with zeolites as ethanol dehydration catalysts).^{38,58} This was true for all NHSG samples in this study (including Sections 3.2 and 3.3).

Conversion improved with the increasing amount of acid sites (Fig. 4 left), the best conversion level being achieved by the catalyst with the highest number of acid sites (**15Si-1MeSi-1Al**). Further increasing the Al loading did not lead to higher activity, probably because sample **15Si-1MeSi-2Al** displayed an abrupt loss of specific surface area, and consequently a loss of accessible acid sites as already discussed. Ethylene selectivity was similar among the NHSG prepared aluminosilicate samples with varying Si:Al ratio (Fig. 4, right, Table 2S).

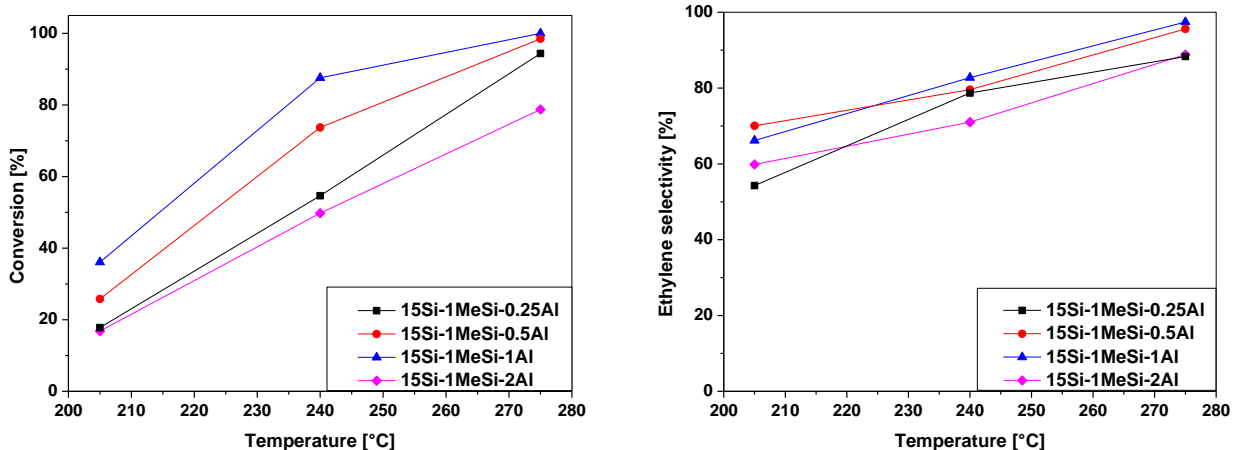


Fig. 4: Ethanol conversion (left) and ethylene selectivity (right) exhibited in gas phase ethanol dehydration by aluminosilicate catalysts with different Si:Al ratio.

Effect of methylation

In order to study the effect of Si-CH₃ groups, a series of hybrid aluminosilicate catalysts with varying Si:MeSi ratio was prepared (**15Si-1MeSi-1Al**, **14Si-2MeSi-1Al**, and **13Si-3MeSi-1Al**). A purely inorganic catalyst (**16Si-1Al**) was prepared as a reference material. The Al loading providing the best catalytic performance was kept constant (Si:Al ratio = 16). The experimental Si:Al ratios (ICP-OES) were close to the nominal values, while the catalyst's surfaces were somewhat richer in Si (XPS, Table 3), similar to the samples with varying Si:Al ratio (Section 3.1).

Textural properties of methylated samples (Table 3) followed a clear trend: specific surface area slightly decreased with the increasing methyl group content (290 m² g⁻¹ vs. 250 m² g⁻¹ for **16Si-1Al** and **13Si-3MeSi-1Al**, respectively). The total pore volume decreased more markedly with the increase in methyl content (from 0.95 to 0.56 cm³ g⁻¹). This in turn led to a decrease of the average pore size (13 nm vs. 8.7 nm for **16Si-1Al** and **13Si-3MeSi-1Al**, respectively). Similar

effects were observed in other sol-gel studies (both hydrolytic and non-hydrolytic); the porosity loss was explained by a lower cross-linking of prepared gels upon introduction of precursors with lower connectivity.^{59,60}

Table 3: Characterization of NHSG prepared samples with different methyl groups loading: Si:Al ratio (theoretical^a, bulk – ICP-OES and surface – XPS), surface area, pore volume, and average pore size estimated from N₂ physisorption experiments, and MeSi groups content based on quantitative ²⁹Si MAS NMR data (in [at%] based on Si molar amount).

Sample	Si:Al ratio	S _{BET} (m ² g ⁻¹)	V _{total} (cm ³ g ⁻¹)	D (nm)
	Theor ^a /ICP/XP S (-)			
16Si-1Al	16.2/17.5/30.0	290	0.95	13
15Si-1MeSi-1Al	15.7/16.3/24.2	270	0.75	11
14Si-2MeSi-1Al	15.5/17.2/27.8	270	0.68	10
13Si-3MeSi-1Al	15.8/14.1/24.5	250	0.56	8.7
15Si-1MeSi-1DAI	16.3/15.9/17.0	390	1.0	10

^aThe nominal Si:Al ratio is 16 in all cases; the theoretical value presented in the table is the value calculated from the precise masses of reactants introduced during the synthesis (n_{Si} , n_{RSi} , n_{Al} , n_{DIPE}), as presented in Table 1S.

IR spectroscopy gave very similar results for the whole series of methylated samples; the most intense absorption bands come from the vibrations of the aluminosilicate matrix (for details see previous section and ESI). Importantly, the increasing intensity of the absorption bands at 1281, 2920, and 2977 cm⁻¹ (δ_s SiCH₃, ν_s CH₃, and ν_{as} CH₃) unambiguously confirmed the presence of increasing amount of Si-CH₃ groups in the series from **15Si-1MeSi-1Al** to **13Si-3MeSi-1Al** (Fig. 5).^{44,45} These absorption bands were not observed in the case of pure inorganic (benchmark) sample **16Si-1Al**. Moreover, the progressive substitution of Si-OH groups (O-H stretch at 3473 cm⁻¹) with Si-CH₃ groups (C-H asymmetric and symmetric stretch at 2977 and 2919 cm⁻¹, respectively) upon increasing the methylation degree is evident.⁶¹⁻⁶³

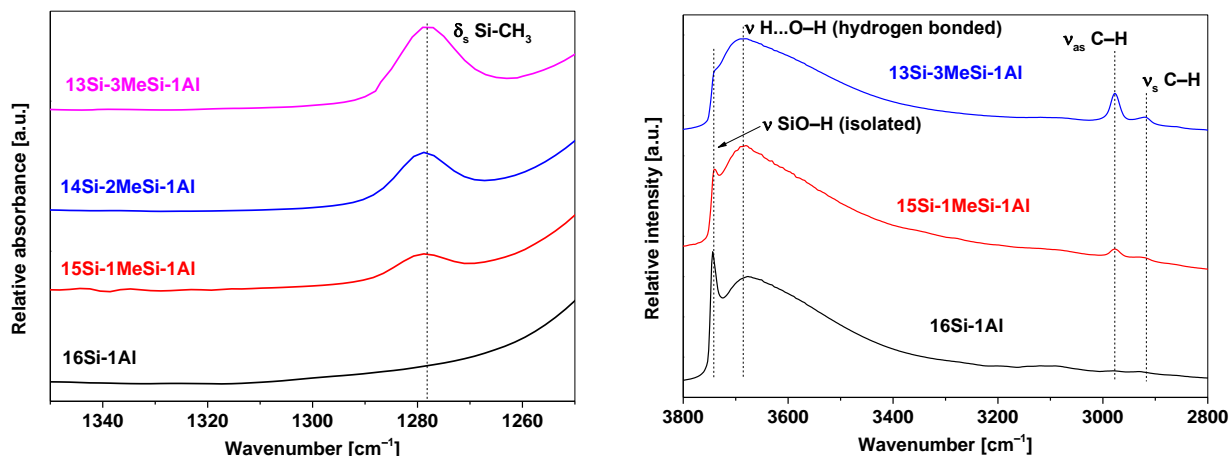


Fig. 5: IR spectra of methylated aluminosilicate catalysts with different Si-CH₃ groups loading. Left: Region showing absorption band of δ_s Si-CH₃ vibration. Right: Region showing absorption bands of stretching vibrations of OH (isolated at 3743 cm⁻¹ and hydrogen bonded at 3679 cm⁻¹) and CH bonds (asymmetric and symmetric at 2977 and 2919 cm⁻¹).

Consistently, in ²⁹Si MAS NMR, the signal at -62 ppm originating from T species was gaining in intensity as the methyl content was increased (Fig. 10S). These spectra were integrated in order to gain a quantitative evaluation of the Si-CH₃ groups content (T vs. Q species). Results are presented in Table 3S as a relative percentage of CH₃SiO₃ species out of all Si moieties. It can be seen, that 53 % of the nominal methyl groups content was retained within the **13Si-3MeSi-1Al** (10 at% experimental vs. 18.8 at% theoretical). The rest was probably lost during the calcination step. **15Si-1MeSi-1Al** and **14Si-2MeSi-1Al** gave very similar results: 55 and 56 % retained MeSi groups, respectively (these values are however only indicative considering the low MeSi groups content and thus a potentially large error during spectra processing).

While IR and NMR spectroscopy have shown the successful incorporation of Si-CH₃ groups within the bulk of the samples, XPS and ToF-SIMS provides information on the organic groups

present at the catalyst surface. Such information is crucial, considering the decisive role played by the surface in heterogeneous catalysis. In XPS spectra (Fig. 11S), a gradual increase in C content was observed for **15Si-1MeSi-1Al**, **14Si-2MeSi-1Al**, and **13Si-3MeSi-1Al** in comparison to **16Si-1Al** (the latter only exhibits the carbon contamination usually encountered in XPS measurement on aluminosilicate materials). Importantly, this trend was clearly caused by the C-(C,H) component of the carbon peak (understand CH₃ groups in this case), which grew markedly in intensity. The contribution of the other oxidized carbon types typically found in carbon contamination remained fairly constant (Fig. 11S, Table 4S).

In ToF-SIMS, several secondary ions related to the presence of the organic groups could be detected: CH₂⁺, CH₃⁺, SiCH₂⁺, SiCH₃⁺, and C₃H₇⁺ (Table 5S and Fig. 12S–15S). Most of these signals was well resolved, without any overlap, and undoubtedly assigned; the only exception was peak of SiCH₃⁺ moieties which was overlapped by some other signals (Fig. 12S). Relative peak areas (calculated as the peak intensity for the considered ion divided by the total count) for SiCH₂⁺ ions (m/z = 41.986) are taken as an indication of the degree of methylation in the surface layer (Fig. 6, left). Clearly, these values were significantly higher for the hybrid catalysts as compared to the inorganic reference (displaying this peak due to a carbon contamination similar to XPS). This gradual increase in relative peak areas was also observed for CH₂⁺ and CH₃⁺ ions (Fig. 13S and 14S). A slight discrepancy in this trend was observed for SiCH₃⁺ ion only (Table 5S). This can, however, be explained due to the presence of overlapping peaks in the mass spectra (Fig. 12S). At the same time, the level of carbon contamination can be estimated following relative peak areas of bigger organic moieties (e.g. C₃H₇⁺). Unlike the four masses discussed above as a proxy for methylation, the masses associated with carbon contamination remained fairly constant

(Fig. 15S). Thus, XPS and ToF-SIMS confirmed the successful incorporation of Si-CH₃ groups which are also present at the outermost surface of the NHSG-prepared aluminosilicates, where it can be expected that they affect the catalytic behavior.

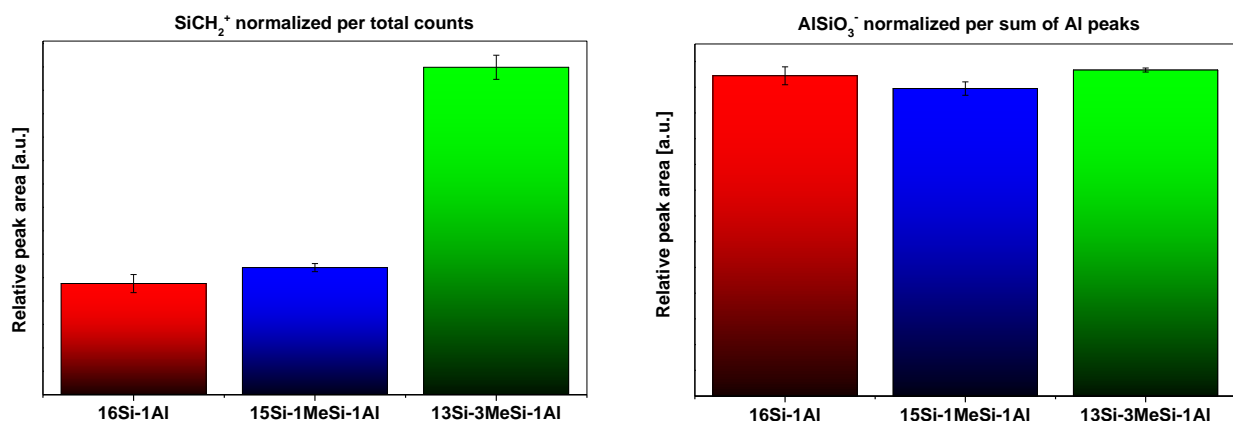


Fig. 6: Comparison of samples with different Si-CH₃ groups loading in terms of relative peak areas of masses corresponding to SiCH₂⁺ ions (representing Si-CH₃ groups) and in terms of relative peak areas of masses corresponding to AlSiO₃⁻ ions (mixed Al-Si clusters) in mass spectra obtained by ToF-SIMS.

The homogeneity of Al mixing within silica matrices was further studied using ToF-SIMS. Peaks of (AlSiO₃)⁻ were followed at $m/z = 102.94$ and taken as an indication of the presence of dispersed Al species incorporated in the silica matrix (Fig. 6, right, Table 5S). This signal was well resolved, without any overlap, and undoubtedly assigned (Fig. 16S). Clearly, the samples with different amounts of MeSi groups show similar (slightly fluctuating) content of mixed Al-Si clusters; no trend was observed. Thus, the homogeneity of Si-Al mixing is similar among the samples with different degree of methylation and, importantly, does not deteriorate with increasing amount of methyl groups. The same conclusion can be drawn from the relative peak areas of other relevant Al containing peaks (e.g. AlSi₂O₅⁻ in Fig. 17S).

In ^{27}Al MAS NMR spectra (Fig. 7, left), a very intense signal of AlO_4 species was observed, accompanied by a less intense band originating from AlO_6 moieties. A higher intensity of the AlO_6 moieties signal was observed for the sample with higher MeSi groups content. To reveal whether this originates from a less thorough incorporation of Al in the silica matrix, additional ^{27}Al MAS NMR experiments were performed on dehydrated samples contacted with pyridine. These analyses (Fig. 7, right) revealed the virtual disappearance of octahedrally coordinated Al atoms in the whole series of methylated samples upon sample dehydration and pyridine adsorption. Thus, it can be stated that the formation of alumina oligomers or particles did not occur in NHSG catalysts whatever the degree of methylation. The AlO_6 species that disappear upon dehydration and pyridine adsorption can be described as isolated surface aluminum species (octahedrally coordinated when hydrated, but tetrahedrally coordinated when coordinated by pyridine), i.e. they work effectively as Lewis acids.

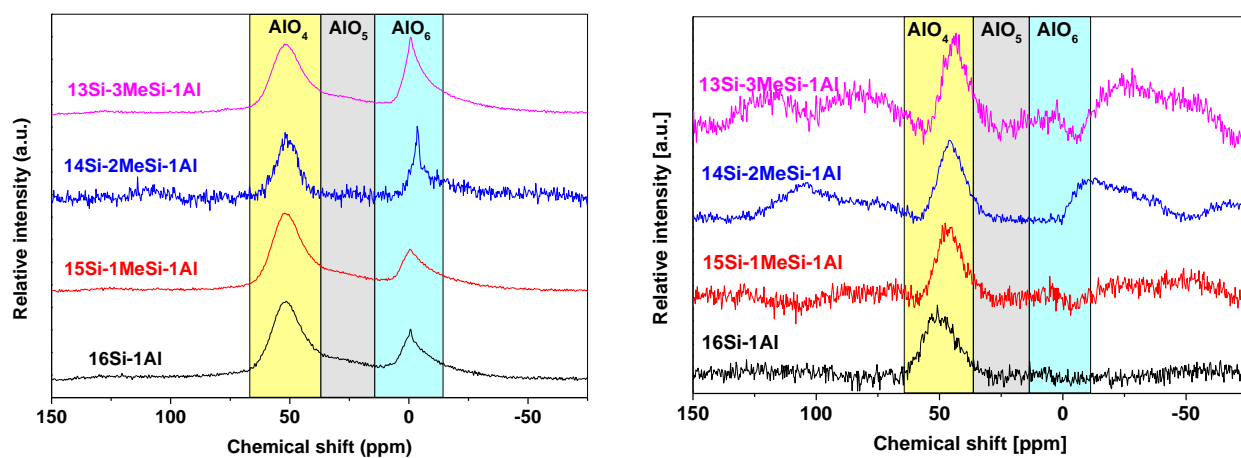


Fig. 7: ^{27}Al MAS NMR spectra of NHSG prepared samples with different Si-CH₃ groups loading. Left: Samples exposed to ambient atmosphere (hydrated); Right: Dehydrated samples with adsorbed pyridine.

IR spectroscopy combined with pyridine adsorption was tentatively used for the estimation of acid sites number, nature, and strength (Table 4). A fair comparison of samples with different degree of methylation was, however, not possible because the spectra baselines in the relevant region (1400–1500 cm^{-1}) were largely affected by the presence of methyl groups – the CH_3 deformation vibration at 1412 cm^{-1} grew in intensity upon increasing methyl groups content (Fig. 18S). Thus, while the data suggest a much lower acidity for the sample with the highest degree of methylation, this does not correlate with other observations, including catalytic evaluation (see below). We suggest, that the number of acid sites based on IR spectroscopy combined with pyridine adsorption is underestimated for methylated samples. Therefore, NH_3 -TPD analyses were performed to describe the amount and strength of acid sites. The results were similar for the samples with different degree of methylation and for the purely inorganic one (Table 4, Fig. 19S).

Table 4: Amount, strength, and nature of acid sites in NHSG prepared aluminosilicates with different Si- CH_3 groups content by pyridine adsorption combined with IR spectroscopy and NH_3 -TPD (last column only).

Sample	Total acid sites [mmol g^{-1}] ^a	B/L ratio [-]	Acid sites after desorption at 350 °C [%]	B/L ratio ^b [-]	Total acid sites ^c [mmol g^{-1}]
16Si-1Al	0.035	0.83	72	0.17	0.254
15Si-1MeSi-1Al	0.035	0.40	70	0.16	0.262
13Si-3MeSi-1Al	0.007	0.37	76	0.46	0.253
15Si-1MeSi-1DAI	0.086	0.40	80	0.11	-

^aWe suggest these data are biased by the fact that the baseline is strongly affected by the methylation degree (see also Fig. 18S), ^bAfter desorption at 350 °C; ^cEstimated by NH_3 -TPD. Note: in NH_3 -TPD and IR-pyridine, it should be recalled that the basic probes differ markedly (pK_b values and steric demands) and the conditions (pressure, temperature) under which the titration of acid sites is done are also completely

different, meaning that direct quantitative comparison should only be made between samples analyzed by the same technique.

Pristine and hybrid catalysts seem to exhibit acid sites of similar strength (~70-76 % of kept pyridine after evacuation at 350 °C, see Table 4). On the contrary, the proportion of Brønsted acid sites is reproducibly and significantly higher in the case of **16Si-1Al** as compared to the methylated catalysts. Since Brønsted acidity in amorphous aluminosilicates is known to originate from pseudo-bridging Si–OH...Al bridges, where Al atom has to act as a Lewis acid,^{63–65} it is logical that the substitution of surface Si–OH groups with Si–CH₃ moieties (Fig. 5) leads to a lower B/L ratio in the case of hybrid aluminosilicates. It is worth noting that the lower B/L ratio for hybrid catalysts in comparison to **16Si-1Al** is in a good agreement with the results of ²⁷Al MAS NMR spectroscopy, where the amount of Lewis acidic surface Al species (octahedrally coordinated when hydrated but tetrahedrally coordinated when dehydrated and coordinated by pyridine) is higher for methylated catalysts (Fig. 7).

Unexpectedly, water adsorption measurements did not show a clear-cut effect of Si–CH₃ groups loading. The methylated samples exhibited only a slight variation in water uptakes, both in absolute and relative values. Here, it should be recalled that the textural properties remain similar when the methyl groups content is modified, meaning that proper comparisons can be made. The “hydrophilicity index” calculated at $p/p_0 = 0.3$ is reported in Fig. 8 (and for the whole range of p/p_0 in Fig. 8S). Interestingly, the water uptake is higher for the hybrid sample **15Si-1MeSi-1Al** than for pure inorganic **16Si-1Al**; then it flutters for **14Si-2MeSi-1Al** and finally it slightly decreases for the sample with the highest MeSi groups content (**13Si-3MeSi-1Al**) (Fig. 8,

Fig. 8S). These variations in hydrophilicity, however, are very small compared to the large effects observed upon changing the Si:Al ratio (Fig. 3 and 8S). Moreover, the steep H₂O uptake at low relative pressure ($p/p_0 < 0.1$) was not modified upon methylation (Fig. 20S). Thus, while the introduction of hydrophobic Si-CH₃ groups at the expense of hydrophilic isolated hydroxogroups on aluminosilicates (as confirmed by IR spectroscopy, Fig. 5) was expected to lead to enhanced hydrophobicity, such effect is not verified experimentally via water sorption. On the one hand, this potential hydrophobization effect may be too small to be detected and the hydrophilic character of the aluminosilicate remains mostly governed by the Si:Al ratio. On the other hand, it is possible that the overall measurement is also influenced by another effect of methylation: the hybrid aluminosilicates contain a higher amount of Lewis acid sites as compared to the purely inorganic **16Si-1Al** catalyst (vide supra). After degassing, these coordinatively unsaturated hydrophilic Lewis acid sites coordinate H₂O molecules (as corroborated by IR-pyridine and ²⁷Al MAS NMR). Arguably, this may explain why **15Si-1MeSi-1Al** appears more hydrophilic than the pristine inorganic catalyst. These results are somewhat similar to those reported by Bispo et al.³ and show that the presence of methyl groups on the surface of aluminosilicates does not necessarily lead to a higher hydrophobicity. On the contrary, the presence of Si-CH₃ moieties can increase the numbers of coordinatively unsaturated Al species (i.e. Lewis acid sites) which attract water and this translates in a higher hydrophilicity.

The water contact angles were recorded in order to complement the water sorption experiments (on samples contacted with ambient air and pelletized). Aluminosilicate catalysts with varying CH₃Si groups content were all found to be highly hydrophilic, with water contact

angles in the 22-34° range. While a gradual increase in the contact angle is observed when increasing the methyl group (Fig. 21S), this effect is very moderate. Consistent with water sorption measurements, no drastic hydrophobization is evidenced in the series of methylated catalysts.

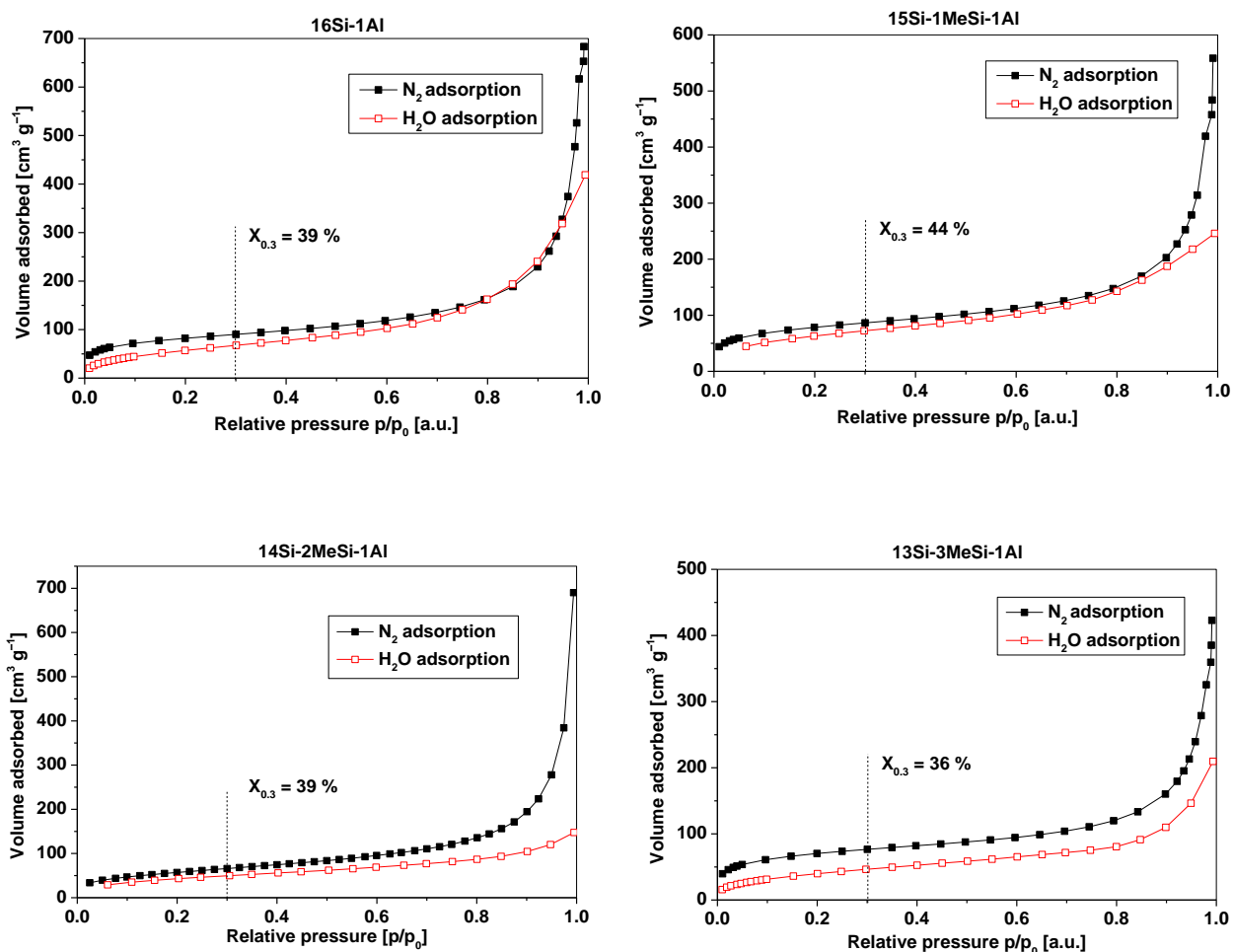


Fig. 8: Comparison of N_2 and H_2O adsorption isotherms for samples with different Si- CH_3 groups loading. „Hydrophilicity index“ $X_{0.3}$ was calculated as a ratio of volume of adsorbed liquid H_2O and volume of adsorbed liquid N_2 at 0.3 p/p_0 ³².

Catalytic performance was compared in this sample series with different degree of methylation (Fig. 9 and Table 2S). On one hand, the ethanol conversion was virtually identical throughout the sample series including the pure inorganic **16Si-1Al**. On the other hand, a pronounced improvement in ethylene selectivity was observed for the hybrid materials, leading to higher ethylene yields. For example, at 240°C, the ethylene yield was 60 % with the pristine inorganic catalyst but reached 73–77 % with the methylated catalysts (Table 2S). These positive effects on selectivity should not be explained by a direct effect of surface hydrophobicity since neither water sorption and nor contact angle measurements reveal any clear hydrophobization of the catalysts which all remain undoubtedly hydrophilic. On the other hand, it should be highlighted that, compared to the pristine inorganic catalyst, the hybrid catalysts contain significantly less Brønsted acid sites (due to a lower Si–OH groups content) and significantly more Lewis acid sites. We propose that this effect is responsible for the increase in ethylene selectivity.

In fact, both Lewis and Brønsted acid sites have been shown to be active in ethanol dehydration.^{51,58} Correspondingly, two possible reaction pathways have been proposed: the direct ethanol dehydration to ethylene and the indirect path starting with dehydration to diethylether followed by its decomposition to ethylene.^{51,66–68} Although the study of reaction mechanisms is beyond the scope of this report we attempted to support the statement that the higher ethylene selectivity correlates with the higher number of Lewis acid sites in hybrid samples. Plots of specific activity at 205 °C (low conversion regime) vs. number of total, Lewis, or Brønsted acid sites (based on IR-pyridine analyses) are shown in Fig. 22S for both ethylene (left) and diethylether (right). On one hand, the specific productivity for diethylether (mmol diethylether per g of catalysts per s) follows the acid site numbers. The quality of the fit is very

good and similar no matter whether total, Lewis, or Brønsted acid sites are considered (Fig. 22S, right), showing that both Lewis and Brønsted acid sites are active in agreement with the literature.^{51,58} On the other hand, the correlations between specific productivity for ethylene (mmol ethylene per g of catalyst per s) and amount of acid sites (total, Lewis, and Brønsted) reveal marked differences. Unambiguously, the best fit was observed with the amount of Lewis acid sites (Fig. 22S, left). The fact that NHSG hybrid catalysts have a higher specific activity for ethylene is in agreement with previous reports showing that aluminosilicates displaying low B/L ratios and strong Lewis acid sites originating in isolated but not fully embedded Al species reached high ethylene selectivity (at the expense of diethyl ether).^{38,51,69}

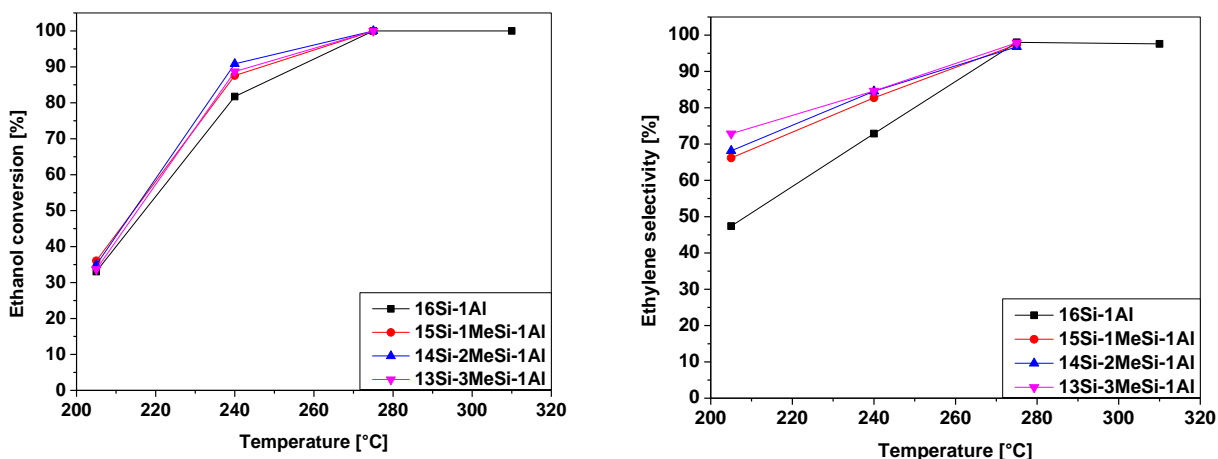


Fig. 9: Ethanol conversion (left) and ethylene selectivity (right) exhibited in gas phase ethanol dehydration by aluminosilicate catalysts with different Si-CH₃ groups loading.

In section 3.1, it was pointed out, neither butenes nor acetaldehyde was formed during catalytic reactions with NHSG aluminosilicate catalysts. These by-products can polymerize easily, form coke, and contribute to catalyst deactivation.^{66,70-74} The absence of coking was confirmed by comparison of TGA curves of fresh and spent catalysts: the shapes of the curves (Fig. 23S) as

well as total mass losses were very similar for samples **16Si-1Al**, **15Si-1MeSi-1Al**, and **13Si-3MeSi-1Al** before and after catalytic tests (Table 6S). These results are in line with previous report studying similar NHSG aluminosilicate catalysts in ethanol dehydration.³⁸ Although coking was discarded on the basis of TGA results, it must be mentioned that the catalysts were not very stable on the long run (Fig. 24S). During a 15h test on stream, both conversion and ethylene selectivity dropped down markedly (conversion by 9.9–26.9 %, ethylene selectivity by 6.7–18.5 %, Table 6S). Modifying the CH₃Si groups content or the Al content did not have any positive effect on stability (Fig. 24S). The progressive deactivation can be associated with the deterioration of textural properties (Table 6S), as discussed in a previous study on NHSG-made aluminosilicate catalysts prepared by alkylhalide elimination, ether route.³⁸ An alternative NHSG route – based on acetamide elimination – was identified as a promising way to solve this issue, and we suggest this should be the object of future studies for hybrid aluminosilicate catalysts.

Delayed Al addition

As discussed in Section 3.2, even a low degree of methylation enabled to improve the already relatively high ethylene selectivity of NHSG-made aluminosilicate catalysts. However, the number of acid sites in aluminosilicate catalysts markedly improved the ethanol conversion (Section 3.1 Si:Al ratio). Further improvement of catalytic performance could be anticipated if one succeeds in increasing the amount of acid sites number while controlling their nature (more Lewis) and strength. While it was possible to increase the number of acid sites and improve catalytic performance by decreasing the Si:Al ratio from 64 to 16, further decrease to 8 did not lead to formation of a higher number of accessible acid sites due to the abrupt loss of specific

surface area. Therefore we introduced a different strategy to boost the amount of surface acid sites: the delayed Al addition to the reaction mixture during the NHSG process. Similar strategies have been proposed in classic (hydrolytic) sol-gel chemistry (where it is based on silicon alkoxides prehydrolysis and helps to improve the homogeneity of Si/M mixing and/or increase the metal loading on the sample surface)⁷⁵ but it is here applied for the first time in NHSG.

The synthesis of **15Si-1MeSi-1Al** was repeated, but in this case, only 10% of the Al precursor was introduced in the sol-gel process from the beginning (a catalytic amount of Al is needed to speed up the polycondensation reactions⁷⁶), and the rest was added 8 hours later. This catalyst is denoted **15Si-1MeSi-1DAI**, where “D” stands for “delayed addition” (experimental details and precise reactant masses can be found in Table 1S).

The textural properties were improved: for **15Si-1MeSi-1DAI**, S_{BET} increased by 43 % to $390 \text{ m}^2 \text{ g}^{-1}$, V_{total} by 33 % to $1.0 \text{ cm}^3 \text{ g}^{-1}$, as compared to **15Si-1MeSi-1Al**, and the average pore diameter remained high (10 nm; Table 3). XPS confirmed that surface Al concentration was higher for the sample with delayed addition of Al precursor (Si:Al ratio 17.0 vs. 24.2, Table 3). IR (Fig. 2S) and SS NMR spectra (Fig. 25S) did not reveal any significant difference between **15Si-1MeSi-1Al** and **15Si-1MeSi-1DAI** suggesting that Al was again thoroughly incorporated in the silica matrix. Importantly, the delayed addition of the Al precursor provoked a marked increase in the number of accessible acid sites (more than doubling, from $0.035 \text{ mmol g}^{-1}$ for **15Si-1MeSi-1Al** to $0.086 \text{ mmol g}^{-1}$ for **15Si-1MeSi-1DAI**; see Table 4, Fig. 5S and 6S). At the same time the nature and strength of the acid sites remained very similar to **15Si-1MeSi-1Al**, both in terms of B/L ratio and in terms of strength (Table 4).

The enhanced acid properties were reflected in markedly higher catalytic performance (Fig. 10, Table 2S). The ethanol conversion increased significantly while maintaining high ethylene selectivity. As a result, sample **15Si-1MeSi-1DAI** markedly outperformed both commercial silica alumina catalyst support (SACS) and γ -alumina. More importantly, looking at the data at 205°C where the catalysts are still far from full conversion, **15Si-1MeSi-1DAI** reaches a higher ethylene yield than the state-of-the-art crystalline zeolite HZSM-5 (37.4 vs. 26.4 %; Table 2S). Thus, the delayed Al addition led to a significantly improved catalytic performance of NHSG-prepared hybrid catalysts and unambiguously confirmed the decisive role of number of acid sites in ethanol dehydration.

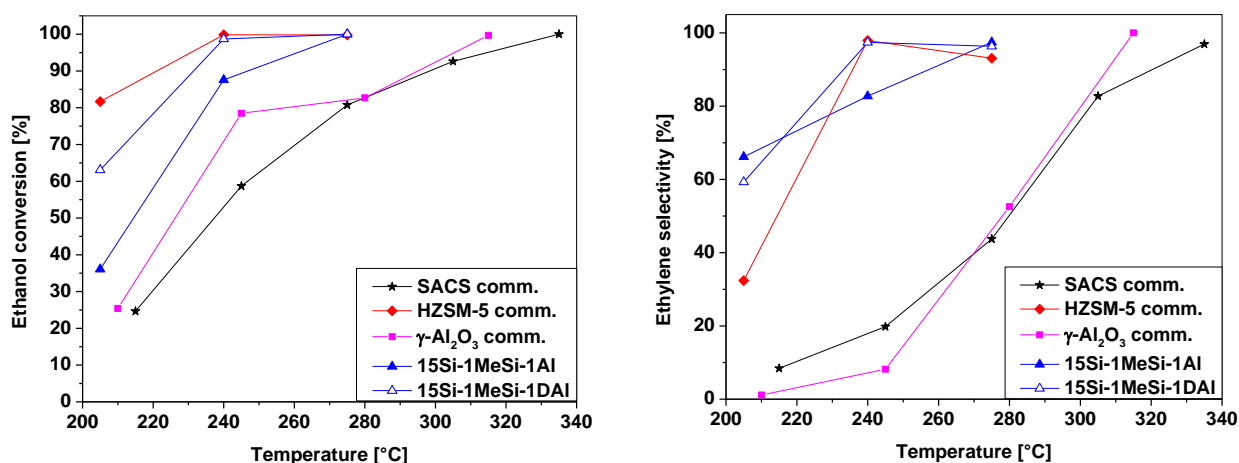


Fig. 10: Ethanol conversion and ethylene selectivity of NHSG prepared aluminosilicate catalysts and commercial benchmarks in ethanol dehydration.

Conclusions

In summary, we have studied hybrid aluminosilicates containing Si-CH₃ groups prepared by a one-pot non-hydrolytic sol-gel route. Si:Al ratio (**15Si-1MeSi-0.25Al-15Si-1MeSi-2Al**) and Si-CH₃

groups content (**16Si-1Al-13Si-3MeSi-1Al**) were varied and the effect on structure, Al speciation, surface properties, number, strength, and nature of acid sites, and catalytic performance in ethanol dehydration were followed. The dispersion of Al was highly homogeneous (up to Si:Al ratio = 16 and whatever the Si-CH₃ groups content) as confirmed by ²⁷Al MAS NMR spectroscopy (no AlO₆ species in dehydrated samples) and ToF-SIMS analyses. The Si-CH₃ groups were successfully incorporated within the aluminosilicate matrices as confirmed by IR, XPS, ToF-SIMS and MAS NMR studies. These materials were highly porous, reaching up to 390 m² g⁻¹ and 1.1 cm³ g⁻¹, even if no sacrificial template was used in the synthesis. The number of acid sites strongly depended on the Si:Al ratio and can be controlled up to Si/Al = 16. Unexpectedly, the introduction of Si-CH₃ groups had no clear-cut effect on the surface hydrophilicity/phobicity as probed by water adsorption and water contact angle measurements. In fact, based on water sorption on degassed sample, some methylated catalysts even appear to be *more hydrophilic* as compared to the pristine inorganic catalyst. While the introduction of Si-CH₃ groups did not lead to a marked change in number of acid sites, it led to decrease in the Brønsted/Lewis acid sites ratio (probably due to a lower Si-OH groups content which were substituted by Si-CH₃ groups). According to ²⁷Al MAS NMR experiments a higher number of Al atoms can be reversibly transformed from octahedral to tetrahedral coordination upon dehydration/hydration in samples with a higher Si-CH₃ groups content (i.e. they work as hydrophilic Lewis acid sites).

Data acquired during the catalytic tests confirmed that the number of acid sites plays a major role in ethanol dehydration: the higher the acid site number, the better the catalytic performance. On the contrary, a direct effect of hydrophilicity/hydrophobicity on catalytic

performance seems improbable. Yet, the hybrid samples provided better ethylene yields than the fully inorganic catalyst mainly due to improved ethylene selectivity. The data suggest that this improvement is caused by a decrease in B/L ratio upon Si-CH₃ groups introduction rather than by an influence of hydrophilicity/hydrophobicity.

Finally, we were able to increase the number of acid sites on purpose by delaying the addition of the Al precursor into the reaction mixture during synthesis (**15Si-1MeSi-1DAI**). The number of acid sites more than doubled while keeping other properties similar to the other NHSG prepared samples. In a good agreement with our conclusion on a crucial effect of number of acid sites on catalytic performance, this catalyst exhibited a marked improvement in ethanol conversion while maintaining high ethylene selectivity and was rivalling highly active HZSM-5 in terms of ethylene yield.

Funding Sources

Marie Skłodowska-Curie grant agreement No 751774.

F.R.S.–F.N.R.S project "EQP U.N030.18.

Communauté française de Belgique, ARC programme 15/20-069.

Czech Science Foundation, project number GJ20-03636Y.

Notes

The authors declare no competing financial interest.

Acknowledgements

A.S. acknowledges funding from the European Union's Horizon 2020 research and innovation programme under the Marie Skłodowska-Curie grant agreement No 751774. F.R.S.–F.N.R.S. is thanked for the acquisition of the physi-chemisorption equipment used here (project "EQP U.N030.18"). Authors acknowledge the 'Communauté française de Belgique' for the financial support through the ARC programme (15/20-069). This research used resources of the "Plateforme Technologique Physico-Chemical Characterization" – PC², the SIAM platform (Synthesis, Irradiation & Analysis of Materials) and the MORPH-IM platform (Morphology & Imaging) located at the University of Namur. The work has been financially supported by the Czech Science Foundation under the project GJ20-03636Y. D.P. Debecker thanks the Francqui Foundation for his "Francqui Research Professor" chair. F. Devred and J.F. Statsyns are acknowledged for the logistical and technical help. We thank Dr. T. Homola and J. Vida for water contact angle measurements.

References

- (1) Faustini, M.; Nicole, L.; Ruiz-Hitzky, E.; Sanchez, C. History of Organic-Inorganic Hybrid Materials: Prehistory, Art, Science, and Advanced Applications. *Adv. Funct. Mater.* **2018**, *28* (27), 1704158. <https://doi.org/10.1002/adfm.201704158>.
- (2) De Clippel, F.; Dusselier, M.; Van De Vyver, S.; Peng, L.; Jacobs, P. A.; Sels, B. F. Tailoring Nanohybrids and Nanocomposites for Catalytic Applications. *Green Chem.* **2013**, *15* (6), 1398–1430. <https://doi.org/10.1039/c3gc37141g>.
- (3) Bispo, C.; Ferreira, P.; Trouvé, A.; Batonneau-Gener, I.; Liu, F.; Jérôme, F.; Bion, N. Role of Acidity and Hydrophobicity in the Remarkable Catalytic Activity in Water of Sulfonic Acid-Functionalized Phenyl-PMO Materials. *Catal. Today* **2013**, *218–219*, 85–92. <https://doi.org/10.1016/j.cattod.2013.06.004>.
- (4) An, S.; Sun, Y.; Song, D.; Zhang, Q.; Guo, Y.; Shang, Q. Arenesulfonic Acid-Functionalized Alkyl-Bridged Organosilica Hollow Nanospheres for Selective Esterification of Glycerol with Lauric Acid to Glycerol Mono- and Dilaurate. *J. Catal.* **2016**, *342*, 40–54. <https://doi.org/10.1016/j.jcat.2016.07.004>.
- (5) Sánchez-Vázquez, R.; Pirez, C.; Iglesias, J.; Wilson, K.; Lee, A. F.; Melero, J. A. Zr-Containing Hybrid Organic-Inorganic Mesoporous Materials: Hydrophobic Acid Catalysts for Biodiesel Production. *ChemCatChem* **2013**, *5* (4), 994–1001. <https://doi.org/10.1002/cctc.201200527>.
- (6) Smeets, V.; Ben Mustapha, L.; Schnee, J.; Gaigneaux, E. M.; Debecker, D. P. Mesoporous SiO₂-TiO₂ Epoxidation Catalysts: Tuning Surface Polarity to Improve Performance in the Presence of Water. *Mol. Catal.* **2018**, *452*, 123–128. <https://doi.org/10.1016/j.mcat.2018.04.011>.
- (7) Lorret, O.; Lafond, V.; Mutin, P. H.; Vioux, A. One-Step Synthesis of Mesoporous Hybrid Titania–Silica Xerogels for the Epoxidation of Alkenes. *Chem. Mater.* **2006**, *18* (20), 4707–4709.

<https://doi.org/10.1021/cm061478q>.

- (8) Melero, J. A.; van Grieken, R.; Morales, G. Advances in the Synthesis and Catalytic Applications of Organosulfonic-Functionalized Mesoporous Materials. *Chem. Rev.* **2006**, *106* (9), 3790–3812. <https://doi.org/10.1021/cr050994h>.
- (9) Gounder, R.; Davis, M. E. Monosaccharide and Disaccharide Isomerization over Lewis Acid Sites in Hydrophobic and Hydrophilic Molecular Sieves. *J. Catal.* **2013**, *308*, 176–188. <https://doi.org/10.1016/j.jcat.2013.06.016>.
- (10) Vivian, A.; Fusaro, L.; Debecker, D. P.; Aprile, C. Mesoporous Methyl-Functionalized Sn-Silicates Generated by the Aerosol Process for the Sustainable Production of Ethyl Lactate. *ACS Sustain. Chem. Eng.* **2018**, *6* (11), 14095–14103. <https://doi.org/10.1021/acssuschemeng.8b02623>.
- (11) Silvestre-Alberó, J.; Domine, M. E.; Jordá, J. L.; Navarro, M. T.; Rey, F.; Rodríguez-Reinoso, F.; Corma, A. Spectroscopic, Calorimetric, and Catalytic Evidences of Hydrophobicity on Ti-MCM-41 Silylated Materials for Olefin Epoxidations. *Appl. Catal. A Gen.* **2015**, *507* (SEPTEMBER), 14–25. <https://doi.org/10.1016/j.apcata.2015.09.029>.
- (12) Dacquin, J. P.; Cross, H. E.; Brown, D. R.; Düren, T.; Williams, J. J.; Lee, A. F.; Wilson, K. Interdependent Lateral Interactions, Hydrophobicity and Acid Strength and Their Influence on the Catalytic Activity of Nanoporous Sulfonic Acid Silicas. *Green Chem.* **2010**, *12* (8), 1383–1391. <https://doi.org/10.1039/c0gc00045k>.
- (13) Behrens, M.; Datye, A. K. *Catalysis for the Conversion of Biomass and Its Derivatives*; Edition open access; Ed. Open Access: Berlin, 2013.
- (14) Angelici, C.; Weckhuysen, B. M.; Bruijninx, P. C. A. Chemocatalytic Conversion of Ethanol into Butadiene and Other Bulk Chemicals. *ChemSusChem* **2013**, *6* (9), 1595–1614. <https://doi.org/10.1002/cssc.201300214>.

- (15) Sun, J.; Wang, Y. Recent Advances in Catalytic Conversion of Ethanol to Chemicals. *ACS Catal.* **2014**, *4* (4), 1078–1090. <https://doi.org/10.1021/cs4011343>.
- (16) Debecker, D. P.; Boissière, C.; Laurent, G.; Huet, S.; Eliaers, P.; Sanchez, C.; Backov, R. First Acidic Macro-Mesocellular Aluminosilicate Monolithic Foams “SiAl(HIPE)” and Their Catalytic Properties. *Chem. Commun.* **2015**, *51* (74), 14018–14021. <https://doi.org/10.1039/C5CC05328E>.
- (17) Gérardy, R.; Debecker, D. P.; Estager, J.; Luis, P.; Monbaliu, J.-C. M. Continuous Flow Upgrading of Selected C₂–C₆ Platform Chemicals Derived from Biomass. *Chem. Rev.* **2020**, *acs.chemrev.9b00846*. <https://doi.org/10.1021/acs.chemrev.9b00846>.
- (18) Zhang, M.; Yu, Y. Dehydration of Ethanol to Ethylene. *Ind. Eng. Chem. Res.* **2013**, *52* (28), 9505–9514. <https://doi.org/10.1021/ie401157c>.
- (19) Fan, D.; Dai, D. J.; Wu, H. S. Ethylene Formation by Catalytic Dehydration of Ethanol with Industrial Considerations. *Materials (Basel)*. **2013**, *6* (1), 101–115. <https://doi.org/10.3390/ma6010101>.
- (20) Shen, J. G. C.; Herman, R. G.; Klier, K. Sulfonic Acid-Functionalized Mesoporous Silica: Synthesis, Characterization, and Catalytic Reaction of Alcohol Coupling to Ethers. *J. Phys. Chem. B* **2002**, *106* (39), 9975–9978. <https://doi.org/10.1021/jp020131h>.
- (21) Sow, B.; Hamoudi, S.; Hassan Zahedi-Niaki, M.; Kaliaguine, S. 1-Butanol Etherification Over Sulfonated Mesostructured Silica and Organo-Silica. *Microporous Mesoporous Mater.* **2005**, *79* (1–3), 129–136. <https://doi.org/10.1016/j.micromeso.2004.10.038>.
- (22) Liu, J.; Yang, J.; Li, C.; Yang, Q. Catalytic Applications of Sulfonic Acid Functionalized Mesoporous Organosilicas with Different Fraction of Organic Groups in the Pore Wall. *J. Porous Mater.* **2009**, *16* (3), 273–281. <https://doi.org/10.1007/s10934-008-9197-8>.

- (23) van Grieken, R.; Melero, J. A.; Morales, G. Etherification of Benzyl Alcohols with 1-Hexanol over Organosulfonic Acid Mesostructured Materials. *J. Mol. Catal. A Chem.* **2006**, *256* (1–2), 29–36. <https://doi.org/10.1016/j.molcata.2006.04.040>.
- (24) Styskalik, A.; Kordoghli, I.; Poleunis, C.; Delcorte, A.; Aprile, C.; Fusaro, L.; Debecker, D. P. Highly Porous Hybrid Metallosilicate Materials Prepared by Non-Hydrolytic Sol-Gel: Hydrothermal Stability and Catalytic Properties in Ethanol Dehydration. *Microporous Mesoporous Mater.* **2020**, *297*, 110028. <https://doi.org/10.1016/j.micromeso.2020.110028>.
- (25) Styskalik, A.; Skoda, D.; Barnes, C. E.; Pinkas, J. The Power of Non-Hydrolytic Sol-Gel Chemistry: A Review. *Catalysts* **2017**, *7* (6), 168. <https://doi.org/10.3390/catal7060168>.
- (26) Debecker, D. P.; Hulea, V.; Mutin, P. H. Mesoporous Mixed Oxide Catalysts via Non-Hydrolytic Sol-Gel: A Review. *Appl. Catal. A Gen.* **2013**, *451*, 192–206. <https://doi.org/10.1016/j.apcata.2012.11.002>.
- (27) Debecker, D. P.; Mutin, P. H. Non-Hydrolytic Sol-Gel Routes to Heterogeneous Catalysts. *Chem. Soc. Rev.* **2012**, *41* (9), 3624–3650. <https://doi.org/10.1039/C2CS15330K>.
- (28) Emeis C. A. Determination of Integrated Molar Extinction Coefficients for Infrared Absorption Bands of Pyridine Adsorbed on Solid Acid Catalysts. *Journal of Catalysis*. 1993, pp 347–354.
- (29) Rouquerol, J.; Rouquerol, F.; Sing, K. S. W. *Adsorption by Powders and Porous Solids*; Academic Press, 1998.
- (30) Lowell, S. *Characterization of Porous Solids and Powders: Surface Area, Pore Size and Density*; Springer, 2004.
- (31) Olson, D. H.; Haag, W. O.; Borghard, W. S. Use of Water as a Probe of Zeolitic Properties: Interaction of Water with HZSM-5. *Microporous Mesoporous Mater.* **2000**, *35–36*, 435–446.

[https://doi.org/10.1016/S1387-1811\(99\)00240-1](https://doi.org/10.1016/S1387-1811(99)00240-1).

- (32) Thommes, M.; Mitchell, S.; Pérez-Ramírez, J. Surface and Pore Structure Assessment of Hierarchical MFI Zeolites by Advanced Water and Argon Sorption Studies. *J. Phys. Chem. C* **2012**, *116* (35), 18816–18823. <https://doi.org/10.1021/jp3051214>.
- (33) Shirley, D. A. High-Resolution X-Ray Photoemission Spectrum of the Valence Bands of Gold. *Phys. Rev. B* **1972**, *5* (12), 4709–4714. <https://doi.org/10.1103/PhysRevB.5.4709>.
- (34) Bouchmella, K.; Stoyanova, M.; Rodemerck, U.; Debecker, D. P.; Hubert Mutin, P. Avoiding Rhenium Loss in Non-Hydrolytic Synthesis of Highly Active Re-Si-Al Olefin Metathesis Catalysts. *Catal. Commun.* **2015**, *58*, 183–186. <https://doi.org/10.1016/j.catcom.2014.09.024>.
- (35) Andrianainarivelo, M.; Corriu, R.; Leclercq, D.; Mutin, P. H.; Vioux, A. Mixed Oxides SiO₂–ZrO₂ and SiO₂–TiO₂ by a Non-Hydrolytic Sol–Gel Route. *J. Mater. Chem.* **1996**, *6* (10), 1665–1671. <https://doi.org/10.1039/JM9960601665>.
- (36) Debecker, D. P.; Bouchmella, K.; Delaigle, R.; Eloy, P.; Poleunis, C.; Bertrand, P.; Gaigneaux, E. M.; Mutin, P. H. One-Step Non-Hydrolytic Sol-Gel Preparation of Efficient V₂O₅-TiO₂ Catalysts for VOC Total Oxidation. *Appl. Catal., B* **2010**, *94* (1–2), 38–45. <https://doi.org/10.1016/j.apcatb.2009.10.018>.
- (37) Caetano, B. L.; Rocha, L. A.; Molina, E.; Rocha, Z. N.; Ricci, G.; Calefi, P. S.; de Lima, O. J.; Mello, C.; Nassar, E. J.; Ciuffi, K. J. Cobalt Aluminum Silicate Complexes Prepared by the Non-Hydrolytic Sol–Gel Route and Their Catalytic Activity in Hydrocarbon Oxidation. *Appl. Catal. A Gen.* **2006**, *311* (1–2), 122–134. <https://doi.org/10.1016/j.apcata.2006.06.028>.
- (38) Styskalik, A.; Vykoukal, V.; Fusaro, L.; Aprile, C.; Debecker, D. P. Mildly Acidic Aluminosilicate Catalysts for Stable Performance in Ethanol Dehydration. *Appl. Catal. B Environ.* **2020**, 118926. <https://doi.org/10.1016/j.apcatb.2020.118926>.

- (39) Crouzet, L.; Leclercq, D.; Mutin, P. H.; Vioux, A. Organic-Inorganic Materials by Nonhydrolytic Sol-Gel Processes: Organosilsesquioxane-Metal Oxide Hybrids. *J. Sol-Gel Sci. Technol.* **2003**, *26* (1–3), 335–338. <https://doi.org/10.1023/A:1020792208751>.
- (40) Kriesel, J. W.; Sander, M. S.; Tilley, T. D. Block Copolymer-Assisted Synthesis of Mesoporous, Multicomponent Oxides by Nonhydrolytic, Thermolytic Decomposition of Molecular Precursors in Nonpolar Media. *Chem. Mater.* **2001**, *13* (10), 3554–3563. <https://doi.org/10.1021/cm010068t>.
- (41) Hirata, Y.; Sakeda, K.; Matsushita, Y.; Shimada, K.; Ishihara, Y. Characterization and Sintering Behavior of Alkoxide-Derived Aluminosilicate Powders. *J. Am. Ceram. Soc.* **1989**, *72* (6), 995–1002. <https://doi.org/10.1111/j.1151-2916.1989.tb06258.x>.
- (42) Ruiz de Sola, E.; Estevan, F.; Torres, F. J.; Alarcón, J. Effect of Thermal Treatment on the Structural Evolution of 3:2 and 2:1 Mullite Monophasic Gels. *J. Non. Cryst. Solids* **2005**, *351* (14–15), 1202–1209. <https://doi.org/10.1016/j.jnoncrysol.2005.02.017>.
- (43) Blackwell, C. S. Investigation of Zeolite Frameworks by Vibrational Properties. 1. The Double-Four-Ring in Group 3 Zeolites. *J. Phys. Chem.* **1979**, *83* (25), 3251–3257. <https://doi.org/10.1021/j100488a014>.
- (44) Handke, M.; Kowalewska, A. Siloxane and Silsesquioxane Molecules - Precursors for Silicate Materials. In *Spectrochimica Acta - Part A: Molecular and Biomolecular Spectroscopy*; Elsevier, 2011; Vol. 79, pp 749–757. <https://doi.org/10.1016/j.saa.2010.08.049>.
- (45) Song, Y.; Huang, Y.; Havenga, E. A.; Butler, I. S. Vibrational Spectra of Crystalline Tetrakis(Trimethylsilyl)Silane(IV), Si[Si(CH₃)₃]₄, at High Pressures. *Vib. Spectrosc.* **2001**, *27* (2), 127–134. [https://doi.org/10.1016/S0924-2031\(01\)00126-6](https://doi.org/10.1016/S0924-2031(01)00126-6).
- (46) Toba, M.; Mizukami, F.; Niwa, S.; Sano, T.; Maeda, K.; Shoji, H. Effect of Preparation Methods on Properties of Amorphous Alumina/Silicas. *J. Mater. Chem.* **1994**, *4* (7), 1131–1135.

- (47) Hayase, G.; Kanamori, K.; Hasegawa, G.; Maeno, A.; Kaji, H.; Nakanishi, K. A Superamphiphobic Macroporous Silicone Monolith with Marshmallow-like Flexibility. *Angew. Chemie Int. Ed.* **2013**, *52* (41), 10788–10791. <https://doi.org/10.1002/anie.201304169>.
- (48) Wang, Z.; Jiang, Y.; Lafon, O.; Trébosc, J.; Duk Kim, K.; Stampfl, C.; Baiker, A.; Amoureux, J.-P.; Huang, J. Brønsted Acid Sites Based on Penta-Coordinated Aluminum Species. *Nat. Commun.* **2016**, *7* (December), 13820. <https://doi.org/10.1038/ncomms13820>.
- (49) Van Bokhoven, J. A.; Van der Eerden, A. M. J.; Koningsberger, D. C. Three-Coordinate Aluminum in Zeolites Observed with in Situ x-Ray Absorption near-Edge Spectroscopy at the Al K-Edge: Flexibility of Aluminum Coordinations in Zeolites. *J. Am. Chem. Soc.* **2003**, *125* (24), 7435–7442. <https://doi.org/10.1021/ja0292905>.
- (50) Styskalik, A.; Abbott, J. G.; Orick, M. C.; Debecker, D. P.; Barnes, C. E. Synthesis, Characterization and Catalytic Activity of Single Site, Lewis Acidic Aluminosilicates. *Catal. Today* **2018**, No. November, 1–9. <https://doi.org/10.1016/j.cattod.2018.11.079>.
- (51) Wang, Z.; O'Dell, L. A.; Zeng, X.; Liu, C.; Zhao, S.; Zhang, W.; Gaborieau, M.; Jiang, Y.; Huang, J. Insight into Three-Coordinate Aluminum Species on Ethanol-to-Olefin Conversion over ZSM-5 Zeolites. *Angew. Chemie Int. Ed.* **2019**, *58* (50), 18061–18068. <https://doi.org/10.1002/anie.201910987>.
- (52) Ng, E. P.; Mintova, S. Nanoporous Materials with Enhanced Hydrophilicity and High Water Sorption Capacity. *Microporous Mesoporous Mater.* **2008**, *114* (1–3), 1–26. <https://doi.org/10.1016/j.micromeso.2007.12.022>.
- (53) Zhang, K.; Lively, R. P.; Noel, J. D.; Dose, M. E.; McCool, B. A.; Chance, R. R.; Koros, W. J. Adsorption of Water and Ethanol in MFI-Type Zeolites. *Langmuir* **2012**, *28* (23), 8664–8673. <https://doi.org/10.1021/la301122h>.

- (54) Wei, J.; Zou, L.; Li, J. Fabrication of Mesoporous Solid Acid Catalysts with Tunable Surface Wettability for Efficient Catalysis. *New J. Chem.* **2016**, *40* (5), 4775–4780.
<https://doi.org/10.1039/C5NJ03445K>.
- (55) Wang, X.; Zhang, Y.; Luo, W.; Elzatahry, A. A.; Cheng, X.; Alghamdi, A.; Abdullah, A. M.; Deng, Y.; Zhao, D. Synthesis of Ordered Mesoporous Silica with Tunable Morphologies and Pore Sizes via a Nonpolar Solvent-Assisted Stober Method. *Chem. Mater.* **2016**, *28* (7), 2356–2362.
<https://doi.org/10.1021/acs.chemmater.6b00499>.
- (56) Wang, B.; Han, H.; Ge, B.; Ma, J.; Zhu, J.; Chen, S. An Efficient Hydrophobic Modification of TS-1 and Its Application in the Epoxidation of Propylene. *New J. Chem.* **2019**, *43* (26), 10390–10397.
<https://doi.org/10.1039/c9nj01937e>.
- (57) Manayil, J.; Lee, A.; Wilson, K. Functionalized Periodic Mesoporous Organosilicas: Tunable Hydrophobic Solid Acids for Biomass Conversion. *Molecules* **2019**, *24* (2), 239.
<https://doi.org/10.3390/molecules24020239>.
- (58) Phung, T. K.; Proietti Hernández, L.; Lagazzo, A.; Busca, G. Dehydration of Ethanol over Zeolites, Silica Alumina and Alumina: Lewis Acidity, Brønsted Acidity and Confinement Effects. *Appl. Catal. A Gen.* **2015**, *493*, 77–89. <https://doi.org/10.1016/j.apcata.2014.12.047>.
- (59) Al-Oweini, R. Surface Characterization by Nitrogen Adsorption of Silica Aerogels Synthesized from Various Si(OR)₄ and R''Si(OR')₃ Precursors. *Appl. Surf. Sci.* **2010**, *257* (1), 276.
- (60) Styskalik, A.; Skoda, D.; Moravec, Z.; Babiak, M.; Barnes, C. E.; Pinkas, J. Control of Micro/Mesoporosity in Non-Hydrolytic Hybrid Silicophosphate Xerogels. *J. Mater. Chem. A* **2015**, *3* (14), 7477–7487. <https://doi.org/10.1039/c4ta06823h>.
- (61) Trombetta, M.; Busca, G.; Rossini, S.; Piccoli, V.; Cornaro, U.; Guercio, A.; Catani, R.; Willey, R. J. FT-IR Studies on Light Olefin Skeletal Isomerization Catalysis. *J. Catal.* **1998**, *179* (2), 581–596.

<https://doi.org/10.1006/jcat.1998.2251>.

- (62) Hensen, E. J. M.; Poduval, D. G.; Ligthart, D. A. J. M.; Van Veen, J. A. R.; Rigutto, M. S. Quantification of Strong Brønsted Acid Sites in Aluminosilicates. *J. Phys. Chem. C* **2010**, *114* (18), 8363–8374. <https://doi.org/10.1021/jp9106348>.
- (63) Hensen, E. J. M.; Poduval, D. G.; Degirmenci, V.; Ligthart, D. A. J. M.; Chen, W.; Maugé, F.; Rigutto, M. S.; Veen, J. A. R. Van. Acidity Characterization of Amorphous Silica-Alumina. *J. Phys. Chem. C* **2012**, *116* (40), 21416–21429. <https://doi.org/10.1021/jp309182f>.
- (64) Leydier, F.; Chizallet, C.; Chaumonnot, A.; Digne, M.; Soyer, E.; Quoineaud, A. A.; Costa, D.; Raybaud, P. Brønsted Acidity of Amorphous Silica-Alumina: The Molecular Rules of Proton Transfer. *J. Catal.* **2011**, *284* (2), 215–229. <https://doi.org/10.1016/j.jcat.2011.08.015>.
- (65) Chizallet, C. Towards the Atomic Scale Simulation of Intricate Acidic Aluminosilicate Catalysts. *ACS Catal.* **2020**. <https://doi.org/10.1021/acscatal.0c01136>.
- (66) Phillips, C. B.; Datta, R. Production of Ethylene from Hydrous Ethanol on H-ZSM-5 under Mild Conditions. *Ind. Eng. Chem. Res.* **1997**, *36* (11), 4466–4475. <https://doi.org/10.1021/ie9702542>.
- (67) Phung, T. K.; Busca, G. Diethyl Ether Cracking and Ethanol Dehydration: Acid Catalysis and Reaction Paths. *Chem. Eng. J.* **2015**, *272*, 92–101. <https://doi.org/10.1016/j.cej.2015.03.008>.
- (68) Zhou, X.; Wang, C.; Chu, Y.; Xu, J.; Wang, Q.; Qi, G.; Zhao, X.; Feng, N.; Deng, F. Observation of an Oxonium Ion Intermediate in Ethanol Dehydration to Ethene on Zeolite. *Nat. Commun.* **2019**, *10* (1), 1–9. <https://doi.org/10.1038/s41467-019-09956-7>.
- (69) Phung, T. K.; Busca, G. Ethanol Dehydration on Silica-Aluminas: Active Sites and Ethylene/Diethyl Ether Selectivities. *Catal. Commun.* **2015**, *68*, 110–115. <https://doi.org/10.1016/J.CATCOM.2015.05.009>.

- (70) Nash, C. P.; Ramanathan, A.; Ruddy, D. A.; Behl, M.; Gjersing, E.; Griffin, M.; Zhu, H.; Subramaniam, B.; Schaidle, J. A.; Hensley, J. E. Mixed Alcohol Dehydration over Brønsted and Lewis Acidic Catalysts. *Appl. Catal. A Gen.* **2016**, *510*, 110–124.
<https://doi.org/10.1016/j.apcata.2015.11.019>.
- (71) Zhang, X.; Wang, R.; Yang, X.; Zhang, F. Comparison of Four Catalysts in the Catalytic Dehydration of Ethanol to Ethylene. *Microporous Mesoporous Mater.* **2008**, *116* (1–3), 210–215.
<https://doi.org/10.1016/j.micromeso.2008.04.004>.
- (72) Nguyen, T. M.; Le Van Mao, R. Conversion of Ethanol in Aqueous Solution over ZSM-5 Zeolites. *Appl. Catal.* **1990**, *58* (1), 119–129. [https://doi.org/10.1016/S0166-9834\(00\)82282-4](https://doi.org/10.1016/S0166-9834(00)82282-4).
- (73) Bi, J.; Guo, X.; Liu, M.; Wang, X. High Effective Dehydration of Bio-Ethanol into Ethylene over Nanoscale HZSM-5 Zeolite Catalysts. *Catal. Today* **2010**, *149* (1–2), 143–147.
<https://doi.org/10.1016/j.cattod.2009.04.016>.
- (74) Xia, W.; Wang, F.; Mu, X.; Chen, K.; Takahashi, A.; Nakamura, I.; Fujitani, T. Catalytic Performance of H-ZSM-5 Zeolites for Conversion of Ethanol or Ethylene to Propylene: Effect of Reaction Pressure and SiO₂/Al₂O₃ratio. *Catal. Commun.* **2017**, *91*, 62–66.
<https://doi.org/10.1016/j.catcom.2016.12.010>.
- (75) Wu, J. F.; Ramanathan, A.; Snively, W. K.; Zhu, H.; Rokicki, A.; Subramaniam, B. Enhanced Metathesis of Ethylene and 2-Butene on Tungsten Incorporated Ordered Mesoporous Silicates. *Appl. Catal. A Gen.* **2016**, *528*, 142–149. <https://doi.org/10.1016/j.apcata.2016.10.004>.
- (76) Bourget, L.; Corriu, R. J. P.; Leclercq, D.; Mutin, P. H.; Vioux, A. Non-Hydrolytic Sol–Gel Routes to Silica. *J. Non. Cryst. Solids* **1998**, *242* (2–3), 81–91. [https://doi.org/10.1016/S0022-3093\(98\)00789-3](https://doi.org/10.1016/S0022-3093(98)00789-3).